

# Production of the Charmonium States $\chi_{c1}$ and $\chi_{c2}$ in Proton Nucleus Interactions at

$$\sqrt{s} = 41.6 \text{ GeV}$$

(The HERA-B Collaboration)

I. Abt<sup>24</sup>, M. Adams<sup>11</sup>, M. Agari<sup>14</sup>, H. Albrecht<sup>13</sup>, A. Aleksandrov<sup>30</sup>, V. Amaral<sup>9</sup>, A. Amorim<sup>9</sup>, S. J. Aplin<sup>13</sup>, V. Aushev<sup>17</sup>, Y. Bagaturia<sup>13,37</sup>, V. Balagura<sup>23</sup>, M. Bargiotti<sup>6</sup>, O. Barsukova<sup>12</sup>, J. Bastos<sup>9</sup>, J. Batista<sup>9</sup>, C. Bauer<sup>14</sup>, Th. S. Bauer<sup>1</sup>, A. Belkov<sup>12,†</sup>, Ar. Belkov<sup>12</sup>, I. Belotelov<sup>12</sup>, A. Bertin<sup>6</sup>, B. Bobchenko<sup>23</sup>, M. Böcker<sup>27</sup>, A. Bogatyrev<sup>23</sup>, G. Bohm<sup>30</sup>, M. Bräuer<sup>14</sup>, M. Bruinsma<sup>29,1</sup>, M. Bruschi<sup>6</sup>, P. Buchholz<sup>27</sup>, T. Buran<sup>25</sup>, J. Carvalho<sup>9</sup>, P. Conde<sup>2,13</sup>, C. Cruse<sup>11</sup>, M. Dam<sup>10</sup>, K. M. Danielsen<sup>25</sup>, M. Danilov<sup>23</sup>, S. De Castro<sup>6</sup>, H. Deppe<sup>15</sup>, X. Dong<sup>3</sup>, H. B. Dreis<sup>15</sup>, V. Egorytchev<sup>13</sup>, K. Ehret<sup>11</sup>, F. Eisele<sup>15</sup>, D. Emelianov<sup>13</sup>, S. Essenov<sup>23</sup>, L. Fabbri<sup>6</sup>, P. Faccioli<sup>6</sup>, M. Feuerstack-Raible<sup>15</sup>, J. Flammer<sup>13</sup>, B. Fominykh<sup>23,†</sup>, M. Funcke<sup>11</sup>, Ll. Garrido<sup>2</sup>, A. Gellrich<sup>30</sup>, B. Giacobbe<sup>6</sup>, J. Gläsel<sup>21</sup>, D. Goloubkov<sup>13,34</sup>, Y. Golubkov<sup>13,35</sup>, A. Golutvin<sup>23</sup>, I. Golutvin<sup>12</sup>, I. Gorbounov<sup>13,27</sup>, A. Gorišek<sup>18</sup>, O. Gouchtchine<sup>23</sup>, D. C. Goulart<sup>8</sup>, S. Gradl<sup>15</sup>, W. Gradl<sup>15</sup>, F. Grimaldi<sup>6</sup>, J. Groth-Jensen<sup>10</sup>, Yu. Guilitsky<sup>23,36</sup>, J. D. Hansen<sup>10</sup>, J. M. Hernández<sup>30</sup>, W. Hofmann<sup>14</sup>, M. Hohlmann<sup>13</sup>, T. Hott<sup>15</sup>, W. Hulsbergen<sup>1</sup>, U. Husemann<sup>27</sup>, O. Igonkina<sup>23</sup>, M. Ispiryan<sup>16</sup>, T. Jagla<sup>14</sup>, C. Jiang<sup>3</sup>, H. Kapitza<sup>13</sup>, S. Karabekyan<sup>26</sup>, N. Karpenko<sup>12</sup>, S. Keller<sup>27</sup>, J. Kessler<sup>15</sup>, F. Khasanov<sup>23</sup>, Yu. Kiryushin<sup>12</sup>, I. Kisel<sup>24</sup>, E. Klinkby<sup>10</sup>, K. T. Knöpfle<sup>14</sup>, H. Kolanoski<sup>5</sup>, S. Korpar<sup>22,18</sup>, C. Krauss<sup>15</sup>, P. Kreuzer<sup>13,20</sup>, P. Krizan<sup>19,18</sup>, D. Krücker<sup>5</sup>, S. Kupper<sup>18</sup>, T. Kvaratskhelia<sup>23</sup>, A. Lanyov<sup>12</sup>, K. Lau<sup>16</sup>, B. Lewendel<sup>13</sup>, T. Lohse<sup>5</sup>, B. Lomonosov<sup>13,33</sup>, R. Männer<sup>21</sup>, R. Mankel<sup>30</sup>, S. Masciocchi<sup>13</sup>, I. Massa<sup>6</sup>, I. Matchikhilian<sup>23</sup>, G. Medin<sup>5</sup>, M. Medinnis<sup>13</sup>, M. Mevius<sup>13</sup>, A. Michetti<sup>13</sup>, Yu. Mikhailov<sup>23,36</sup>, R. Mizuk<sup>23</sup>, R. Muresan<sup>10</sup>, M. zur Nedden<sup>5</sup>, M. Negodaev<sup>13,33</sup>, M. Nörenberg<sup>13</sup>, S. Nowak<sup>30</sup>, M. T. Núñez Pardo de Vera<sup>13</sup>, M. Ouchrif<sup>29,1</sup>, F. Ould-Saada<sup>25</sup>, C. Padilla<sup>13</sup>, D. Peralta<sup>2</sup>, R. Pernack<sup>26</sup>, R. Pestotnik<sup>18</sup>, B. AA. Petersen<sup>10</sup>, M. Piccinini<sup>6</sup>, M. A. Pleier<sup>14</sup>, M. Poli<sup>6,32</sup>, V. Popov<sup>23</sup>, D. Pose<sup>12,15</sup>, S. Prystupa<sup>17</sup>, V. Pugatch<sup>17</sup>, Y. Pylypchenko<sup>25</sup>, J. Pyrlik<sup>16</sup>, K. Reeves<sup>14</sup>, D. Reßing<sup>13</sup>, H. Rick<sup>15</sup>, I. Riu<sup>13</sup>, P. Robmann<sup>31</sup>, I. Rostovtseva<sup>23</sup>, V. Rybnikov<sup>13</sup>, F. Sánchez<sup>14</sup>, A. Sbrizzi<sup>1</sup>, M. Schmelling<sup>14</sup>, B. Schmidt<sup>13</sup>, A. Schreiner<sup>30</sup>, H. Schröder<sup>26</sup>, U. Schwanke<sup>30</sup>, A. J. Schwartz<sup>8</sup>, A. S. Schwarz<sup>13</sup>, B. Schwenninger<sup>11</sup>, B. Schwingenheuer<sup>14</sup>, F. Sciacca<sup>14</sup>, N. Semprini-Cesari<sup>6</sup>, S. Shuvalov<sup>23,5</sup>, L. Silva<sup>9</sup>, L. Sözüer<sup>13</sup>, S. Solunin<sup>12</sup>, A. Somov<sup>13</sup>, S. Somov<sup>13,34</sup>, J. Spengler<sup>13</sup>, R. Spighi<sup>6</sup>, A. Spiridonov<sup>30,23</sup>, A. Stanovnik<sup>19,18</sup>, M. Starić<sup>18</sup>, C. Stegmann<sup>5</sup>, H. S. Subramania<sup>16</sup>, M. Symalla<sup>13,11</sup>, I. Tikhomirov<sup>23</sup>, M. Titov<sup>23</sup>, I. Tsakov<sup>28</sup>, U. Uwer<sup>15</sup>, C. van Eldik<sup>13,11</sup>, Yu. Vassiliev<sup>17</sup>, M. Villa<sup>6</sup>, A. Vitale<sup>6,7</sup>, I. Vukotic<sup>5,30</sup>, H. Wahlberg<sup>29</sup>, A. H. Walenta<sup>27</sup>, M. Walter<sup>30</sup>, J. J. Wang<sup>4</sup>, D. Wegener<sup>11</sup>, U. Werthenbach<sup>27</sup>, H. Wolters<sup>9</sup>, R. Wurth<sup>13</sup>, A. Wurz<sup>21</sup>, S. Xella-Hansen<sup>10</sup>, Yu. Zaitsev<sup>23</sup>, M. Zavertyaev<sup>13,14,33</sup>, T. Zeuner<sup>13,27</sup>, A. Zhelezov<sup>23</sup>, Z. Zheng<sup>3</sup>, R. Zimmermann<sup>26</sup>, T. Živko<sup>18</sup>, A. Zoccoli<sup>6</sup>

<sup>1</sup>NIKHEF, 1009 DB Amsterdam, The Netherlands <sup>a</sup>

<sup>2</sup>Department ECM, Faculty of Physics, University of Barcelona, E-08028 Barcelona, Spain <sup>b</sup>

<sup>3</sup>Institute for High Energy Physics, Beijing 100039, P.R. China

<sup>4</sup>Institute of Engineering Physics, Tsinghua University, Beijing 100084, P.R. China

<sup>5</sup>Institut für Physik, Humboldt-Universität zu Berlin, D-12489 Berlin, Germany <sup>c,d</sup>

<sup>6</sup>Dipartimento di Fisica dell'Università di Bologna and INFN Sezione di Bologna, I-40126 Bologna, Italy

<sup>7</sup>also from Fondazione Giuseppe Occhialini, I-61034 Fossombrone(Pesaro Urbino), Italy

<sup>8</sup>Department of Physics, University of Cincinnati, Cincinnati, Ohio 45221, USA <sup>e</sup>

<sup>9</sup>LIP Coimbra, P-3004-516 Coimbra, Portugal <sup>f</sup>

<sup>10</sup>Niels Bohr Institutet, DK 2100 Copenhagen, Denmark <sup>g</sup>

<sup>11</sup>Institut für Physik, Universität Dortmund, D-44221 Dortmund, Germany <sup>d</sup>

<sup>12</sup>Joint Institute for Nuclear Research Dubna, 141980 Dubna, Moscow region, Russia

<sup>13</sup>DESY, D-22603 Hamburg, Germany

<sup>14</sup>Max-Planck-Institut für Kernphysik, D-69117 Heidelberg, Germany <sup>d</sup>

<sup>15</sup>Physikalisches Institut, Universität Heidelberg, D-69120 Heidelberg, Germany <sup>d</sup>

<sup>16</sup>Department of Physics, University of Houston, Houston, TX 77204, USA <sup>e</sup>

<sup>17</sup>Institute for Nuclear Research, Ukrainian Academy of Science, 03680 Kiev, Ukraine <sup>h</sup>

<sup>18</sup>J. Stefan Institute, 1001 Ljubljana, Slovenia <sup>i</sup>

<sup>19</sup>University of Ljubljana, 1001 Ljubljana, Slovenia

<sup>20</sup> *University of California, Los Angeles, CA 90024, USA* <sup>j</sup>

<sup>21</sup> *Lehrstuhl für Informatik V, Universität Mannheim, D-68131 Mannheim, Germany*

<sup>22</sup> *University of Maribor, 2000 Maribor, Slovenia*

<sup>23</sup> *Institute of Theoretical and Experimental Physics, 117218 Moscow, Russia* <sup>k</sup>

<sup>24</sup> *Max-Planck-Institut für Physik, Werner-Heisenberg-Institut, D-80805 München, Germany* <sup>d</sup>

<sup>25</sup> *Dept. of Physics, University of Oslo, N-0316 Oslo, Norway* <sup>l</sup>

<sup>26</sup> *Fachbereich Physik, Universität Rostock, D-18051 Rostock, Germany* <sup>d</sup>

<sup>27</sup> *Fachbereich Physik, Universität Siegen, D-57068 Siegen, Germany* <sup>d</sup>

<sup>28</sup> *Institute for Nuclear Research, INRNE-BAS, Sofia, Bulgaria*

<sup>29</sup> *Universiteit Utrecht/NIKHEF, 3584 CB Utrecht, The Netherlands* <sup>a</sup>

<sup>30</sup> *DESY, D-15738 Zeuthen, Germany*

<sup>31</sup> *Physik-Institut, Universität Zürich, CH-8057 Zürich, Switzerland* <sup>m</sup>

<sup>32</sup> *visitor from Dipartimento di Energetica dell' Università di Firenze and INFN Sezione di Bologna, Italy*

<sup>33</sup> *visitor from P.N. Lebedev Physical Institute, 117924 Moscow B-333, Russia*

<sup>34</sup> *visitor from Moscow Physical Engineering Institute, 115409 Moscow, Russia*

<sup>35</sup> *visitor from Moscow State University, 119992 Moscow, Russia*

<sup>36</sup> *visitor from Institute for High Energy Physics, Protvino, Russia*

<sup>37</sup> *visitor from High Energy Physics Institute, 380086 Tbilisi, Georgia*

<sup>†</sup> *deceased*

<sup>a</sup> supported by the Foundation for Fundamental Research on Matter (FOM), 3502 GA Utrecht, The Netherlands

<sup>b</sup> supported by the CICYT contract AEN99-0483

<sup>c</sup> supported by the German Research Foundation, Graduate College GRK 271/3

<sup>d</sup> supported by the Bundesministerium für Bildung und Forschung, FRG, under contract numbers 05-7BU35I, 05-7DO55P, 05-HB1HRA, 05-HB1KHA, 05-HB1PEA, 05-HB1PSA, 05-HB1VHA, 05-HB9HRA, 05-7HD15I, 05-7MP25I, 05-7SI75I

<sup>e</sup> supported by the U.S. Department of Energy (DOE)

<sup>f</sup> supported by the Portuguese Fundação para a Ciência e Tecnologia under the program POCTI

<sup>g</sup> supported by the Danish Natural Science Research Council

<sup>h</sup> supported by the National Academy of Science and the Ministry of Education and Science of Ukraine

<sup>i</sup> supported by the Ministry of Education, Science and Sport of the Republic of Slovenia under contracts number P1-135 and J1-6584-0106

<sup>j</sup> supported by the U.S. National Science Foundation Grant PHY-9986703

<sup>k</sup> supported by the Russian Ministry of Education and Science, grant SS-1722.2003.2, and the BMBF via the Max Planck Research Award

<sup>l</sup> supported by the Norwegian Research Council

<sup>m</sup> supported by the Swiss National Science Foundation

A measurement of the ratio  $R_{\chi_c} = (\chi_c \rightarrow J/\psi + \gamma)/J/\psi$  in pC, pTi and pW interactions at 920 GeV/c ( $\sqrt{s} = 41.6$  GeV) in the Feynman-x range  $-0.35 < x_F^{J/\psi} < 0.15$  is presented. Both  $\mu^+\mu^-$  and  $e^+e^- J/\psi$  decay channels are observed with an overall statistics of about 15000  $\chi_c$  events, which is by far the largest available sample in pA collisions. The result is  $R_{\chi_c} = 0.188 \pm 0.013_{st}^{+0.024}_{-0.022_{sys}}$  averaged over the different materials, when no  $J/\psi$  and  $\chi_c$  polarisations are considered. The  $\chi_{c1}$  to  $\chi_{c2}$  production ratio  $R_{12} = R_{\chi_{c1}}/R_{\chi_{c2}}$  is measured to be  $1.02 \pm 0.40$ , leading to a cross section ratio  $\frac{\sigma(\chi_{c1})}{\sigma(\chi_{c2})} = 0.57 \pm 0.23$ . The dependence of  $R_{\chi_c}$  on the Feynman-x of the  $J/\psi$ ,  $x_F^{J/\psi}$ , and its transverse momentum,  $p_T^{J/\psi}$ , is studied, as well as its dependence on the atomic number, A, of the target. For the first time, an extensive study of possible biases on  $R_{\chi_c}$  and  $R_{12}$  due to the dependence of acceptance on the polarization states of  $J/\psi$  and  $\chi_c$  is performed. By varying the polarisation parameter,  $\lambda_{obs}$ , of all produced  $J/\psi$ 's by two sigma around the value measured by HERA-B, and considering the maximum variation due to the possible  $\chi_{c1}$  and  $\chi_{c2}$  polarisations, it is shown that  $R_{\chi_c}$  could change by a factor between 1.02 and 1.21 and  $R_{12}$  by a factor between 0.89 and 1.16.

PACS numbers:

13.20.Gd Decays of  $J/\psi$ ,  $\Upsilon$  and other quarkonia

13.85.-t Hadron-induced high- and super-high-energy interactions

24.85.+p Quarks, gluons, and QCD in nuclei and nuclear processes

13.88.+e Polarisation in interactions and scattering

## I. INTRODUCTION

Since the discovery of charmonium more than thirty years ago, its production in hadronic collisions has attracted considerable theoretical and experimental interest for a variety of reasons. In particular the question of the production mechanism, which requires an understanding of the hadronisation process in the non-perturbative regime and, in addition, the influence of nuclear matter, are of particular importance since the suppression of  $J/\psi$  production has been considered as a possible indicator of the quark-gluon plasma [1].

The theoretical treatment of quarkonium production is usually broken into two steps: the creation of a heavy quark pair in interactions of the colliding partons, calculable by means of perturbative QCD, and the transition to a bound state, involving poorly understood non-perturbative processes and even more problematic nuclear effects. A variety of approaches have been developed to describe quarkonium production such as the Color Evaporation Model (CEM) [2], the Color Singlet Model (CSM) [3], and non-relativistic QCD (NRQCD) [4]. A measurement of the fraction of  $J/\psi$  coming from the decay of other charmonium states (feed-down) provides useful tests of the model predictions. While a rather rich sample of data on  $J/\psi$  production exists, the available data on the production rates, or even the experimentally simpler fractional production rates, of the other charmonium states suffer from imprecision. Moreover very little experimental information is available on the possible polarisation of the produced charmonium states.

In this paper we report on the production of the charmonium states  $\chi_{c1}$  and  $\chi_{c2}$  in collisions of a 920 GeV proton beam with nuclear targets. The  $\chi_c$  mesons are identified via their radiative decay into  $J/\psi$  mesons which in turn are decaying into lepton pairs. The production and decay chain is:

$$pA \rightarrow \chi_c + X; \quad \chi_c \rightarrow \gamma J/\psi \rightarrow \gamma l^+ l^- \quad (l = e, \mu). \quad (1)$$

To minimise systematic uncertainties the  $\chi_c$  rates are normalised to the total production rate of  $J/\psi$ . We define  $R_{\chi_c}$ , the fraction of  $J/\psi$  originating from radiative  $\chi_c$  decays:

$$R_{\chi_c} = \frac{\sum_{i=1}^2 \sigma(\chi_{ci}) Br(\chi_{ci} \rightarrow J/\psi \gamma)}{\sigma(J/\psi)} \quad (2)$$

where  $Br(\chi_{ci} \rightarrow J/\psi \gamma)$  are the branching ratios for the different  $\chi_{ci} \rightarrow J/\psi \gamma$  decays,  $\sigma(\chi_{ci})$  are their production cross sections per nucleon and  $\sigma(J/\psi)$  is the total  $J/\psi$

production cross section per nucleon. In Tab. I the main properties of the three  $\chi_c$  states ( $\chi_{c0}$ ,  $\chi_{c1}$  and  $\chi_{c2}$ ) are reported. Due to the negligible  $\chi_{c0} \rightarrow J/\psi \gamma$  branching ratio, we limit our study to  $\chi_{c1}$  and  $\chi_{c2}$  production.

State	Mass ( $MeV/c^2$ )	Width ( $MeV/c^2$ )	BR( $\rightarrow J/\psi \gamma$ )
$\chi_{c0}$	$3414.76 \pm 0.35$	$10.4 \pm 0.7$	$(1.30 \pm 0.11)\%$
$\chi_{c1}$	$3510.66 \pm 0.07$	$0.89 \pm 0.05$	$(35.6 \pm 1.9)\%$
$\chi_{c2}$	$3556.20 \pm 0.09$	$2.06 \pm 0.12$	$(20.2 \pm 1.0)\%$

TABLE I: *Properties of the three  $\chi_c$  states [5].*

In Section II an overview of the physics motivations for our measurement is given together with a survey of the existing experimental results. In Section III the experiment and the data taking conditions are described and in Section IV the principle of the measurement is explained. The simulation used for evaluating detection efficiencies and the measurements in the muon and electron decay channels are described in Sections V, VIA and VIB, respectively. In Section VII, the effect of possible  $J/\psi$  and  $\chi_c$  polarisations (not directly measured in this analysis) on  $R_{\chi_c}$  and  $R_{12} = R_{\chi_{c1}}/R_{\chi_{c2}}$  is discussed. A discussion of systematic uncertainties and the final result are given in Sections VIII and IX, respectively.

## II. $\chi_c$ PRODUCTION

### A. QCD Models of Charmonium Production

In the Color Evaporation Model (CEM), charmonium production is described as the creation of  $c\bar{c}$  pairs with an invariant mass below the  $D\bar{D}$  threshold. Their hadronisation is mediated by the emission of soft gluons which do not significantly alter the kinematics of the  $c\bar{c}$  system. The production rates of the various charmonium states are predicted to be proportional to each other and independent of the projectile, target and energy. Most experiments measuring  $R_{\chi_c}$  in proton and pion induced interactions [6]-[21] provide compatible results with the predicted value  $R_{\chi_c} \approx 0.4$  [22]. The assumption of the universality of charmonium hadronisation implies that the value of  $R_{\chi_c}$  should be independent of the kinematic variables  $x_F$  and  $p_T$  of the produced charmonium state [22] ( $x_F$  is the Feynman variable in the nucleon-nucleon center-of-mass system;  $p_T$  is the transverse momentum relative to the incoming beam).

In the Color Singlet Model (CSM), the quark pair is created in a hard scattering reaction as a colour sin-

glet (CS) with the same quantum numbers as the final quarkonium. Since two gluons can form a colourless C-even state such as the  $\chi_c$  states, but at least three gluons are needed to form a colourless C-odd state such as the  $\psi$  states,  $\psi$  production in this model is suppressed by an additional factor  $\alpha_s$ . As a result, the  $J/\psi$  production rate should be dominated by feed-down from radiative  $\chi_c$  decays and  $R_{\chi_c}$  is predicted to be close to 1. Most of the proton induced  $\chi_c$  measurements are in disagreement with this assumption [6]-[14].

In response to the disagreement between the CSM and measurements in most charmonium production features [23], a more generalised perturbative QCD approach for charmonium production, ‘non-relativistic QCD’ (NRQCD), was developed which includes not only  $c\bar{c}$  pairs produced as colour singlets but also as colour octets (CO). The CO states subsequently evolve into the observed charmonium by soft gluon emission. At the HERA-B beam energy of 920 GeV, the dominant production process is  $gg$  fusion which contributes both to CO and CS states. Therefore  $\chi_c$  production dominates the CS part of  $J/\psi$  production while direct  $J/\psi$  and  $J/\psi$  from  $\psi'$  decay are produced via CO states. The predicted ratio,  $R_{\chi_c} \approx 0.3$  [22] is in agreement with most of the existing measurements in proton induced interactions [6]-[14]. NRQCD predicts only small differences in the differential cross sections of the different charmonium states as a function of  $x_F$ , mostly at large values of  $x_F$ . More visible differences can arise when considering nuclear-matter effects (A-dependence) due to the differing absorption probabilities of the various charmonium and pre-charmonium states in nuclei [22].

## B. Interactions with Nucleons and A-dependence

The CEM model and NRQCD differ in their predictions of the suppression of the charmonium production rate per nucleon in interactions with heavy nuclei compared to interactions with single proton targets. Suppression can occur in interactions of the generated  $c\bar{c}$  quarks with nuclear matter which could lead to an  $x_F$  dependence: for  $x_F > 0$ , the formation length of the final charmonium state exceeds the size of the nucleus, while for  $x_F < 0$ , an increasingly larger fraction is formed already inside the nucleus. In the context of the CEM, only one proto-charmonium state exists and thus for  $x_F > 0$ , the differences in suppression between  $J/\psi$ ,  $\psi'$  and the  $\chi_c$  states should be small. For  $x_F < 0$ , the  $\chi_c$  and  $\psi'$  states should be more suppressed than the  $J/\psi$  due to their larger interaction cross sections. In the context of NRQCD, substantial differences in the suppression of the various charmonium states are expected even for  $x_F > 0$  since the wave function of the CO states extends over a much larger distance and the resulting interaction cross section is considerably larger than that of the CS states [22].

## C. $R_{\chi_c}$ and the Quark-Gluon Plasma

The so-called ‘‘anomalous’’ suppression of  $J/\psi$  has been proposed as a possible indicator of the formation of a quark-gluon plasma [1] and such suppression has subsequently been reported by several experiments [24] [25] [26]. Nevertheless the conclusion that the reported suppression is indeed anomalous is contingent on the full understanding of normal suppression mechanisms, i.e. those existing in the absence of a quark-gluon plasma as is expected to be the case in proton-nucleus reactions. In this respect the measurement of the fraction of  $J/\psi$  arising from feed-down decays ( $\chi_c$  and  $\psi'$ ) is important since the anomalous suppression is expected to be sensitive to the mass and binding energy of the different charmonium states. Directly produced  $J/\psi$  survive in the quark-gluon plasma up to about  $1.5 T_c$  [27],  $T_c$  being the critical temperature, while  $\chi_c$  and  $\psi'$  states dissociate just above  $T_c$ . Thus several drops in the distribution of charmonium survival probability as a function of the temperature are expected, with the size of the drops dependant on the fractions  $R_{\chi_c}$  and  $R_{\psi'}$  ( $R_{\psi'} = \frac{\sigma(\psi')Br(\psi' \rightarrow J/\psi X)}{\sigma(J/\psi)}$ ). Experimentally, only the first drop has been reported [24] [25] [26], and is interpreted as indicating the disassociation of  $\chi_c$  and  $\psi'$ . Several models attempt to describe the totality of experimental data on  $J/\psi$  suppression. They generally assume  $R_{\chi_c} \sim 0.3$  and  $R_{\psi'} \sim 0.1$ . Nevertheless all the proposed models fail to simultaneously describe all the existing data, as they all overestimate the suppression unless other effects, such as  $J/\psi$  regeneration, are assumed to describe the RHIC data [27]. From the value of  $R_{\chi_c}$  shown in Sect. IX and the result from [28],  $R_{\psi'} \approx 7\%$ ,  $R_{\chi_c} + R_{\psi'} \approx 0.27$ , which is lower than generally assumed.

## D. Previous Measurements

The production of  $\chi_c$  has been measured both in proton- and pion-induced reactions on various nuclear targets and in  $pp$  and  $p\bar{p}$  interactions [6]-[21]. Tab. II lists all the published measurements of  $\chi_c$  production in hadronic interactions and reports their most relevant features. From this table some observations can be made:

- all fixed target measurements are based on at most a few hundreds  $\chi_c$ ;
- all experiments observe only one of the two  $J/\psi$  decay channels ( $e^+e^-$  or  $\mu^+\mu^-$ );
- the photon efficiency never exceeds 30%;
- most measurements are performed in the positive  $x_F$  range.

Tab. III shows the measured values of  $R_{\chi_c}$  and/or of the  $\chi_c$  cross sections separately for proton and pion induced reactions. The values shown in Figs. 1 and 2 have been

updated using the current PDG values [5] for the  $\chi_c$  and  $J/\psi$  decay branching ratios, and the  $J/\psi$  cross sections obtained from [29].

The available data scatter strongly, well beyond their respective uncertainties, and no energy dependence is discernible. The proton data seem to favour a value  $R_{\chi_c} \sim 0.3$ , supporting the prediction of NRQCD, but the quality of the available data does not allow a firm conclusion.

### III. THE EXPERIMENT AND THE DATA SAMPLE

The HERA-B detector [30] was a forward magnetic spectrometer used to study the interactions of the 920 GeV proton beam ( $\sqrt{s} = 41.6$  GeV) of the HERA accelerator on a variety of nuclear targets. The detector components relevant for this analysis are the wire target system [31] which could be dynamically positioned in the halo of the proton beam, the Silicon Vertex Detector (VDS) [32], the dipole magnet of 2.13 Tm, the drift-tube Tracking System (OTR) [33], the Ring Imaging Cherenkov Counter (RICH) [34], the sampling Electromagnetic Calorimeter (ECAL) [35] and the Muon Detector (MUON) [36].

The data sample of about 160 million events used for this analysis was acquired at an interaction rate of about 5 MHz with a dedicated di-lepton trigger [37] in order to select both  $J/\psi \rightarrow e^+e^-$  and  $J/\psi \rightarrow \mu^+\mu^-$  final states. In total about 300,000  $J/\psi$  were reconstructed, distributed almost equally in the two decay channels. Nine different wire configurations were used, both in single and double wire runs. The wire materials used were carbon (C,  $\approx 64\%$  of the full statistics), tungsten (W,  $\approx 31\%$ ), and titanium (Ti,  $\approx 5\%$ ). Continuous on-line monitoring ensured stable running conditions, and further offline data quality checks were applied to select only runs with properly functioning detector and trigger components.

### IV. EXPERIMENTAL METHOD

$R_{\chi_c}$  is defined in Eq. 2. The quantity to be measured is:

$$R_{\chi_c} = \frac{\frac{N_{\chi_{c1}} \cdot \varepsilon_{J/\psi}^{dir}}{\varepsilon_{\chi_{c1}} \cdot \varepsilon_{\gamma}^{\chi_{c1}}} + \frac{N_{\chi_{c2}} \cdot \varepsilon_{J/\psi}^{dir}}{\varepsilon_{\chi_{c2}} \cdot \varepsilon_{\gamma}^{\chi_{c2}}}}{N_{J/\psi} + \frac{N_{\chi_{c1}}}{\varepsilon_{\gamma}^{\chi_{c1}}} \cdot \left(\frac{\varepsilon_{J/\psi}^{dir}}{\varepsilon_{\chi_{c1}}} - 1\right) + \frac{N_{\chi_{c2}}}{\varepsilon_{\gamma}^{\chi_{c2}}} \cdot \left(\frac{\varepsilon_{J/\psi}^{dir}}{\varepsilon_{\chi_{c2}}} - 1\right)} \quad (3)$$

where  $N_{J/\psi}$  is the total number of observed  $J/\psi$ 's,  $N_{\chi_{c1}}$  ( $N_{\chi_{c2}}$ ) is the number of counted  $\chi_{c1}$ 's ( $\chi_{c2}$ 's),  $\varepsilon_{J/\psi}^{dir}$  is the direct  $J/\psi$  total detection efficiency, including trigger losses, reconstruction and cut selection,  $\varepsilon_{J/\psi}^{\chi_{c1}}$  ( $\varepsilon_{J/\psi}^{\chi_{c2}}$ ) is the total detection efficiency for  $J/\psi$  coming from  $\chi_{c1}$  ( $\chi_{c2}$ ) decay and  $\varepsilon_{\gamma}^{\chi_{c1}}$  ( $\varepsilon_{\gamma}^{\chi_{c2}}$ ) is the identification efficiency

of the photon from  $\chi_{c1}$  ( $\chi_{c2}$ ) decay for events with identified  $J/\psi$ 's. The measurement method consists of evaluating  $N_{J/\psi}$  by analysis of the di-lepton invariant mass spectra and  $N_{\chi_{c1}}$ ,  $N_{\chi_{c2}}$  by analysis of the  $J/\psi$ - $\gamma$  invariant mass spectra, for events with selected  $J/\psi$  candidates. The efficiency terms in Eq. 3 are extracted from the MC simulation.

The production ratio of the two states can be determined using:

$$R_{12} = \frac{R_{\chi_{c1}}}{R_{\chi_{c2}}} = \frac{N_{\chi_{c1}}}{N_{\chi_{c2}}} \cdot \frac{\varepsilon_{J/\psi}^{\chi_{c2}} \cdot \varepsilon_{\gamma}^{\chi_{c2}}}{\varepsilon_{J/\psi}^{\chi_{c1}} \cdot \varepsilon_{\gamma}^{\chi_{c1}}} \quad (4)$$

(where  $R_{\chi_{c1}} + R_{\chi_{c2}} = R_{\chi_c}$ ) and the production cross section ratio can be evaluated using:

$$\frac{\sigma(\chi_{c1})}{\sigma(\chi_{c2})} = R_{12} \frac{Br(\chi_{c2} \rightarrow J/\psi\gamma)}{Br(\chi_{c1} \rightarrow J/\psi\gamma)} \quad (5)$$

In order to perform an internally consistent analysis, the same procedure and cuts are applied to both the  $e^+e^-$  and  $\mu^+\mu^-$  channels except for the lepton particle identification (PID) requirements.

#### A. $J/\psi$ Selection

Leptons from  $J/\psi$  decay are selected from the triggered tracks, re-fitted using offline alignment constants and taking into account multiple scattering when extrapolating to the target. A  $\chi^2$  probability of the track fit  $> 0.3\%$  is required. Additional PID cuts are applied depending on the lepton channel.

In the muon channel, a muon likelihood is constructed from information in the MUON detector and is required to be greater than 5% and a kaon likelihood is constructed from RICH information and required to be less than 99%.

In the electron channel a more complex set of PID cuts is needed. First the calorimeter is searched for a cluster consistent with having been caused by a Bremsstrahlung photon emitted in front of the magnet [35]. Since the presence of such a cluster very effectively identifies electrons, the cut values used for the remaining two particle identification criteria can be substantially relaxed when such a Bremsstrahlung cluster is found. The additional two criteria are a more restrictive matching requirement between the OTR track of the electron candidate and its corresponding ECAL cluster, and a requirement that the track momentum be consistent with the deposited calorimeter energy.

Once opposite sign lepton candidates ( $\mu^+\mu^-$  or  $e^+e^-$ ) are selected, their common vertex is fitted and the  $\chi^2$  probability of the fit is required to be greater than 1%. In a few percent of the events, more than one di-lepton combination pass all cuts, in which case only the one with the lowest product of track-fit  $\chi^2$  is retained. Finally, the invariant mass of the di-lepton pair is calculated and

Exp.	beam/ target	$\sqrt{s}$ GeV	$l^+l^-$	$\gamma$ det.	$\varepsilon_\gamma$ %	$x_F$	$p_T$ GeV/c	$E_\gamma$ cut GeV	$N_{J/\psi}$	$N_{\chi_c}$	$\chi_{ci}$ sep.
ISR [6]	pp	< 55 >	$e^+e^-$	d				> 0.4	658	$31 \pm 11$	n
R702 [7]	pp	52.4,62.7	$e^+e^-$	d			< 3	0.4-0.6	975		n
ISR [8]	pp	62	$e^+e^-$	d			< 5	> 0.4			n
E610 [9]	pBe	19.4,21.7	$\mu^+\mu^-$	d	16	0.1-0.7	< 2	3-50	$157 \pm 17$	$11.8 \pm 5.4$	f
E705 [10]	pLi	23.8	$\mu^+\mu^-$	d	27	-0.1-0.5	0.-0.4	> 1.0	$6090 \pm 90$	$250 \pm 35$	f
E771 [12]	pSi	38.8	$e^+e^-$	c	0.8	> 0.0		0.25-0.7	$11660 \pm 139$	66	y
HERA-B [14]	pC,Ti	41.6	$\{e^+e^-\}_{\mu^+\mu^-}$	d	30	-0.25-0.15		$E_T > 1.0$	$4420 \pm 100$	$370 \pm 74$	n
CDF [11],[13]	$p\bar{p}$	1800	$\mu^+\mu^-$	$\{d\}_c$	$\{15\}$		> 4.0	> 1.0	$\{88000\}_{32642 \pm 185}$	$\{119 \pm 14\}_{1230 \pm 72}$	$\{y\}_n$
E369 [15]	$\pi^- Be, p$	20.2	$\mu^+\mu^-$	d		0-0.8	< 3	< 5	160	$17.2 \pm 6.6$	n
WA11 [16]	$\pi^- Be$	18.7	$\mu^+\mu^-$	c	1				44750	157	y
IHEP140 [17]	$\pi^- p$	8.6	$e^+e^-$	d		> 0.4	< 2	> 2	120	10	n
E673 [18]	$\pi^- Be$	20.6	$\mu^+\mu^-$	d	21			10-25	$1056 \pm 36$	$84 \pm 15$	n
E610 [19]	$\pi^- Be$	18.9	$\mu^+\mu^-$	d	19	0.1-0.7	< 2	3-50	$908 \pm 41$	$53.6 \pm 17.1$	f
E705 [20]	$\{\pi^+ - Li\}$	23.8	$\mu^+\mu^-$	d	27				$\{5560 \pm 90\}_{12470 \pm 160}$	$\{300 \pm 35\}_{590 \pm 50}$	n
E672/706 [21]	$\pi^- Be$	31.1	$\mu^+\mu^-$	$\{d\}_c$	$\{2\}_{11}$	0.1-0.8		> 10	$7750 \pm 110$	$\{379 \pm 66\}_{105 \pm 18}$	$\{f\}_y$

TABLE II: Previous  $R_{\chi_c}$  measurements in hadronic collisions. Symbols:  $\gamma$  detection ( $d$ =direct,  $c$ = $\gamma$ -conversion).  $\chi_{c1}$ - $\chi_{c2}$  separation ( $y$ =yes,  $n$ =no,  $f$ =with 2-states fit).

Exp.	Measured values				Updated values			
	$R_{\chi_c}$	$\frac{\sigma(\chi_{c1})}{\sigma(\chi_{c2})}$	$\sigma(\chi_{c1})$ (nb/n)	$\sigma(\chi_{c2})$ (nb/n)	$R_{\chi_c}$	$\frac{\sigma(\chi_{c1})}{\sigma(\chi_{c2})}$	$\sigma(\chi_{c1})$ (nb/n)	$\sigma(\chi_{c2})$ (nb/n)
[6]	$0.43 \pm 0.21$				$0.43 \pm 0.21$			
[7]	$0.15^{+0.10}_{-0.15}$				$0.15^{+0.10}_{-0.15}$			
[8]	0.47(8)				0.47(8)			
[9]	0.47(23)	0.24(28)	64(81)	268(136)	0.47(23)	0.24(28)	39(49)	162(81)
[10]	0.30(4)	0.08(25)(15)	31(62)(3)	364(124)(36)	0.30(4)	0.09(29)(17)	24(48)(2)	244(83)(16)
[12]	0.77(30)(15)	0.53(20)(7)	526(138)(64)	996(286)(134)	0.76(29)(16)	0.61(24)(4)	488(128)(56)	805(231)(92)
[14]	0.32(6)(4)				0.32(6)(4)			
[11]	0.297(17)(57)	1.04(29)(12)			0.297(17)(57)	1.19(33)(14)		
[15]	0.70(28)				0.70(28)			
[16]	0.30(5)	0.68(28)	65(18)	96(29)	0.30(5)	0.79(28)	58(13)	74(19)
[17]	0.44(16)	1(fix)	28(10)	28(10)	0.44(16)	1(fix)	22(8)	22(8)
[18]	0.37(9)	1.12(42)			0.37(9)	1.11(41)		
[19]	0.31(10)	0.96(64)	130(56)	134(64)	0.31(10)	0.98(74)	102(43)	104(49)
[20]	0.40(4)				0.40(4)			
[20]	0.37(3)	0.70(15)	131(17)	189(31)	0.37(3)	0.80(16)	101(13)	126(19)
[21]	0.443(41)(35)	0.57(16)	464(87)	815(168)	0.443(41)(35)	0.65(18)	356(66)	544(107)

TABLE III:  $R_{\chi_c}$ ,  $\frac{\sigma(\chi_{c1})}{\sigma(\chi_{c2})}$ ,  $\sigma(\chi_{c1})$  and  $\sigma(\chi_{c2})$  results in hadronic collisions. Statistical and systematic uncertainties are shown in brackets (less significant digits). See text for an explanation of the updated values.

required to be within  $2\sigma$  of the nominal  $J/\psi$  mass, with  $\sigma = 36 \text{ MeV}/c^2$  in the muon channel and  $64 \text{ MeV}/c^2$  in the electron channel.

## B. Mass Difference Plot

The next step after  $J/\psi$  selection is the identification of suitable photon candidates. A photon is defined as a reconstructed ECAL cluster [38] with at least three contiguous hit cells. The cluster energy,  $E^\gamma$ , is required to be

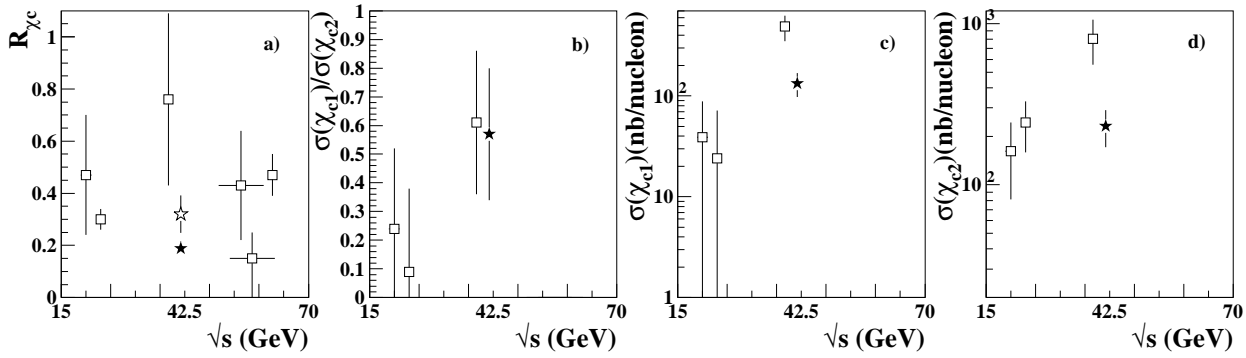


FIG. 1: Summary of experimental results on  $R_{\chi_c}$  (a),  $\frac{\sigma(\chi_{c1})}{\sigma(\chi_{c2})}$  (b),  $\sigma(\chi_{c1})$  (c) and  $\sigma(\chi_{c2})$  (d) in  $pN$  interactions. HERA-B results: open star (old), full star (new).

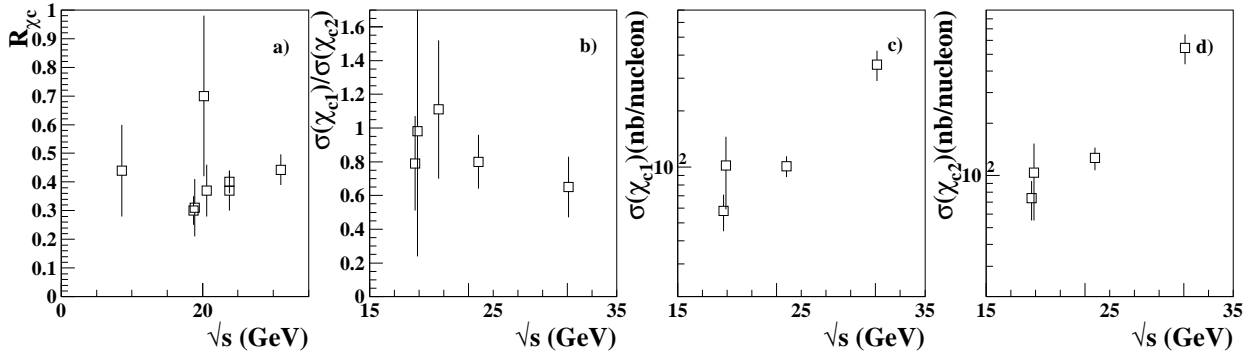


FIG. 2: Summary of experimental results on  $R_{\chi_c}$  (a),  $\frac{\sigma(\chi_{c1})}{\sigma(\chi_{c2})}$  (b),  $\sigma(\chi_{c1})$  (c) and  $\sigma(\chi_{c2})$  (d) in  $\pi N$  interactions.

at least 0.3 GeV and the cluster transverse energy,  $E_T^\gamma$ , is required to be at least 0.2 GeV, for an optimal cluster reconstruction. Furthermore, the ECAL cell with the highest energy deposit of the cluster is required to contain at least 80% of the total cluster energy in order to provide some discrimination against showering hadrons. Clusters which match reconstructed tracks are excluded unless the matching track is formed only from hits behind the magnet and point to the selected di-lepton vertex. Such tracks are mainly from conversions of event-related photons behind the magnet. Finally, because of high background near the proton beam pipe, clusters in an elliptic region around the pipe ( $\sqrt{x_{clust}^2/4 + y_{clust}^2} < 22$  cm, where  $x_{clust}$  and  $y_{clust}$  are the horizontal and vertical positions of the cluster with respect to the beam) are excluded.

Since a photon from a  $\chi_c$  decay cannot be distinguished from the others in the event (on average  $\sim 20$ ), the combinatorial background to the  $\chi_c$  signal is very large, as will be shown in Sect. IV C.

To largely eliminate the uncertainty due to di-lepton mass resolution, the analysis is performed using the mass difference,  $\Delta M = M(J/\psi\gamma) - M(J/\psi)$ . The dominant contribution to the mass difference resolution is the intrinsic photon energy resolution determined by the ECAL.

### C. Background Description

The analysis crucially depends on the background shape being correctly described. We distinguish between “physical” backgrounds (due to the decay of heavier states which include a  $J/\psi$  and one or more photons in their decay products) and “combinatorial” background (due to photons from the event combined with di-leptons which share no parent resonance). The combinatorial background by far dominates. The only significant physical background comes from  $\psi(2S) \rightarrow J/\psi\pi^0\pi^0$  which contributes at the level of  $\approx 15\%$  of the  $\chi_c$  rate but with a rather flat distribution in the  $\Delta M$  spectrum. The shape of this background is estimated from Monte Carlo and subtracted after proper normalisation.

A “Mixed Event” (ME) procedure is adopted for modelling the combinatorial background: a  $J/\psi$  candidate from one event (“event-A”) is mixed with the photons of several ( $\approx 20$ ) other selected events (which we all call “event-B”). Event-B is required to have the same neutral cluster multiplicity as event-A to ensure similar photon energy spectra. Furthermore, the angular difference between the vector sums of transverse momenta of all photons in event-A and event-B is required to be no more than  $2\pi/20$  to ensure the events to be kinematically similar and thus to have similar acceptance.

Extensive tests, both with Monte Carlo and the data itself, were performed to verify the ME procedure. For example, using the data, the combination of photons with  $l^+l^-$  pairs in the  $J/\psi$  side bands (defined as the di-lepton mass intervals outside  $3\sigma$  of the nominal  $J/\psi$  mass, see Sect. IV A) in the SE (“same event”) and with  $l^+l^-$  pairs inside the  $J/\psi$  mass window in the ME spectra show no reflection of the  $\chi_c$  peak and the SE over ME ratio for these events is found to be flat. The normalisation of the ME spectrum is incorporated into the fit of the  $\Delta M$  spectrum as a free parameter (see Sect. VI B).

## V. THE MONTE CARLO SIMULATION

### A. Event generator and detector simulation

In the HERA-B Monte Carlo, the basic process  $pN \rightarrow Q\bar{Q}X$  is simulated, first, by generating the heavy quarks ( $Q\bar{Q}$ ), including hadronisation, with PYTHIA 5.7 [39]; secondly, the energy of the remaining part of the process (X) is given as an input to FRITIOF [40], which is used to simulate the interactions inside the nucleus. PYTHIA describes by default the charmonium production based on the Color Singlet Model. Further colour singlet and colour octet processes were therefore added, according to the NRQCD approach [14]. Differing kinematic distributions for directly produced  $J/\psi$  and  $J/\psi$  from feed-down decays generated according to this model result in slightly different acceptances:  $\sim 78.3\%$  for direct  $J/\psi$  and  $\sim 77.6\%$  for  $J/\psi$  from both  $\chi_{c1}$  and  $\chi_{c2}$ , with no significant difference between the two  $\chi_c$  states.

In the simulation, both direct  $J/\psi$  and  $\chi_c$  states are generated with no polarisation and all results are given under this assumption. The effects of  $J/\psi$  and  $\chi_c$  polarisation are discussed and treated separately (see Sect. VII).

The detector response is simulated using GEANT 3.21 [41] and includes individual detector channel resolutions, noise, efficiencies and calibration precision. The second level trigger algorithm is applied to the simulated detector hits and the first level trigger efficiency is taken from an efficiency map obtained from the data itself. The generated Monte Carlo is reconstructed with the same package used for reconstructing the data and the same analysis cuts are applied to the MC and the data.

In order to check the MC material description, which influences the photon efficiency determination, three different studies were performed by using the Bremsstrahlung tag [35], the  $\pi^0$  signal (where the decay photons are seen as neutral clusters or as converted photons), and the converted photons (see Sect. V B and VIII).

The predicted resolution of the  $\chi_{c1}$  and  $\chi_{c2}$  states is found to be  $\sim 0.032$  GeV/ $c^2$ , in agreement with real data (see Sect. VI B).

### B. $J/\psi$ and photon efficiency

According to Eq. 3, the ratios of efficiencies for  $J/\psi$  coming from the decay of the  $\chi_c$  states to that of directly produced  $J/\psi$  are needed. These ratios are estimated from MC and the values obtained are reported in Table IV. As can be seen from the table, these ratios are independent of target, decay channel and  $\chi_c$  state, within the errors.

The photon detection efficiencies are also evaluated with the MC although an additional correction factor derived from the data was found to be needed, as will be discussed below. For the efficiency evaluation, the same analysis as for the data is performed, but the photon from the  $\chi_c$  decay is selected using MC generation information and checked for acceptance after all cuts are applied. The alternative of extracting the number of  $\chi_c$ ’s from the MC using the ME background subtraction applied to the data, and thus inferring the photon efficiency without recourse to the MC generation information, was found to give a compatible efficiency, but with lower precision.

The MC estimate for photon detection efficiency was checked by comparing the efficiency derived from MC to that, obtained from data, for the detection by the ECAL of reconstructed electrons or positrons from photon conversions before the magnet. Since the average di-lepton triggered data run contains several thousands of such reconstructible conversions, the method affords a detailed check of the stability of photon detection efficiency over the run as well as a check of the MC.

The tracks from the converted photons are required to share a common VDS track segment and to have hits in the OTR chamber immediately before the ECAL (to discriminate against electrons which start to shower before the ECAL). When using the positron from such a pair as a probe, the electron (“tag”) is also required to have an associated ECAL cluster with a deposited energy compatible with the electron track momentum (and vice versa). For selected electron and positron probes, the ECAL is searched for a geometrically matching cluster and the ratio of the deposited ECAL energy to the track momentum (“E/p ratio”) is entered into a histogram. Signal to background ratios of the order of 15 are achieved. The E/p ratio histogram of the probe as well as the corresponding E/p histogram of the tag are fitted to gaussians to describe the signal and third order polynomials for the background description. The fit describes the data well with  $\chi^2$  values typically equal to or less than the number of degrees of freedom. The efficiency is extracted from the fit parameters. The ratio of MC efficiencies estimates to the efficiency derived by this method is found to be  $1.144 \pm 0.034$ , with the quoted uncertainty dominated by run to run variations. Roughly half the difference between efficiency estimates from MC and data can be attributed to a higher ECAL cluster multiplicity in the data compared to the MC – when a cluster caused by a photon from a  $\chi_c$  overlaps with an-



other cluster the photon's measured energy becomes too large and the mass estimate incorrect. The remaining ( $\approx 7\%$ ) discrepancy is not understood but is likely due to cases where the energy deposited by the photon (electron) is considerably less than would be expected from gaussian statistics.

In Tab. V the values of efficiency and the width of  $\chi_{c1}$  and  $\chi_{c2}$  are reported for the two lepton channels and for the different target materials.

Mat.	$\mu^+\mu^-$		$e^+e^-$	
	$\frac{\varepsilon_{J/\psi}^{dir}}{\varepsilon_{\chi_{c1}}}$	$\frac{\varepsilon_{J/\psi}^{dir}}{\varepsilon_{\chi_{c2}}}$	$\frac{\varepsilon_{J/\psi}^{dir}}{\varepsilon_{\chi_{c1}}}$	$\frac{\varepsilon_{J/\psi}^{dir}}{\varepsilon_{\chi_{c2}}}$
C	0.972(7)	0.965(5)	0.970(12)	0.950(7)
W	0.957(8)	0.974(6)	0.985(14)	0.955(9)
Ti	1.008(26)	0.957(17)	-	-

TABLE IV: The ratio of efficiencies for detection of directly produced  $J/\psi$ 's to that of  $J/\psi$ 's coming from  $\chi_{c1}$  and  $\chi_{c2}$  decay. The efficiencies for  $\mu^+\mu^-$  and  $e^+e^-$  channels and for each target material are given separately.

Mat.	$\varepsilon_{\chi_{c1}}^{\gamma}$ (%)	$\sigma_{\chi_{c1}}$ (MeV/c <sup>2</sup> )	$\varepsilon_{\chi_{c2}}^{\gamma}$ (%)	$\sigma_{\chi_{c2}}$ (MeV/c <sup>2</sup> )
C	$40.5 \pm 0.4$	$30.2 \pm 0.4$	$41.2 \pm 0.2$	$33.0 \pm 0.2$
W	$37.1 \pm 0.5$	$32.0 \pm 0.7$	$38.2 \pm 0.3$	$34.3 \pm 0.5$
Ti	$41.3 \pm 1.3$	$31.6 \pm 0.8$	$41.4 \pm 0.8$	$30.2 \pm 0.3$
C	$39.6 \pm 0.6$	$32.1 \pm 0.4$	$40.4 \pm 0.3$	$33.0 \pm 0.2$
W	$38.6 \pm 1.0$	$33.7 \pm 0.8$	$38.3 \pm 0.6$	$35.4 \pm 0.4$

TABLE V: Photon detection efficiencies and the expected widths of  $\Delta M$  peaks for  $\chi_{c1}$  and  $\chi_{c2}$  for the muon (first part) and the electron (second part) channels.

## VI. EVENT COUNTING

### A. $J/\psi$ counting

*a. The muon channel:* The  $\mu^+\mu^-$  invariant mass spectra for C, Ti, and W samples as well as the summed spectrum are shown in Fig. 3 along with a fitted curve. The fit includes the  $J/\psi$  and  $\psi'$  peaks, each described by a superposition of three gaussians with a common mean plus a radiative tail to describe the photon emission process  $\psi \rightarrow \mu^+\mu^-\gamma$  [28], and an exponential to describe the background. The numbers of  $J/\psi$  within the mass window used for  $\chi_c$  selection are reported in Tab. VI.

*b. The electron channel:* The  $e^+e^-$  invariant mass spectra for the different materials and the full sample are shown in Fig. 4. The fit used for the signals ( $J/\psi$  and  $\psi'$ ) includes a Gaussian for the right part of the peaks and, for the left part, a Breit-Wigner to take into account the Bremsstrahlung tail, while a gaussian (exponential)

describes the background in the low (high) mass region with the requirement of continuity of the functions and of the first derivatives. The numbers of  $J/\psi$  within the mass window used for  $\chi_c$  selection are reported in Tab. VI.

### B. $\chi_c$ counting

The  $\Delta M$  spectra are shown in Fig. 5 for the muon channel, and Fig. 6 for the electron channel. In the upper parts of these figures, the SE data are indicated by points. Fits to the ME and SE samples are shown as solid lines. The two curves are not distinguishable except in the  $\Delta M$  region between 0.3 and 0.6 GeV/c<sup>2</sup> where the ME curve is below the SE curve. The fit to the SE spectrum uses the ME parameterization to describe the background and Gaussian distributions for the signal, as described below. In order to evaluate the quality of the background description, the background subtracted spectra are shown below the fitted  $\Delta M$  spectra for visual representation only. A clear  $\chi_c$  signal is visible both in the carbon and tungsten samples, while in the titanium sample, the significance of the  $\chi_c$  signal is at the level of  $\sim 3.5\sigma$  only.

The detector resolution for the two  $\chi_c$  states is comparable with their mass difference, resulting in a single  $\chi_c$  peak in the  $\Delta M$  spectrum. It is nevertheless possible to count separately the number of  $\chi_{c1}$  and  $\chi_{c2}$  (and therefore measure  $R_{12}$ ) by using a fit with two gaussians with some of the parameters fixed, namely:

1.  $\Delta M_{\chi_{c1}} = 0.4137$  GeV/c<sup>2</sup> [5];
2.  $\sigma_{\chi_{c1}}$  fixed according to the MC prediction from Tab V;
3.  $\Delta M(\chi_{c2}) - \Delta M(\chi_{c1}) = 0.0455$  GeV/c<sup>2</sup> [5];
4.  $\frac{\sigma_{\chi_{c2}}}{\sigma_{\chi_{c1}}} = 1.05$  as predicted by MC.

The free parameters are  $N_{\chi_c} = N_{\chi_{c1}+\chi_{c2}}$ ,  $\frac{N_{\chi_{c1}}}{N_{\chi_{c2}}}$  and the ME normalisation parameter. In Tab. VII the values of the fitted  $N_{\chi_c}$  and  $\frac{N_{\chi_{c1}}}{N_{\chi_{c2}}}$  are reported for both the electron and muon channels together with the  $\chi_c$  counting obtained with a single-gaussian fit where the  $\chi_c$  is considered as a single peak.

In order to verify the assumptions made, a systematic study of the effect of releasing the different fixed parameters or varying them within a range around the assumed values was done, as well as a cross check of the  $\chi_c$  counting with the signal modelled as a single gaussian to describe both  $\chi_c$  states. The results of these studies are discussed in Sect. VIII.

## VII. POLARISATION

The experimental determination of polarisation can be used to probe assumptions on the impact of specific QCD processes and the influence of nuclear effects. The data

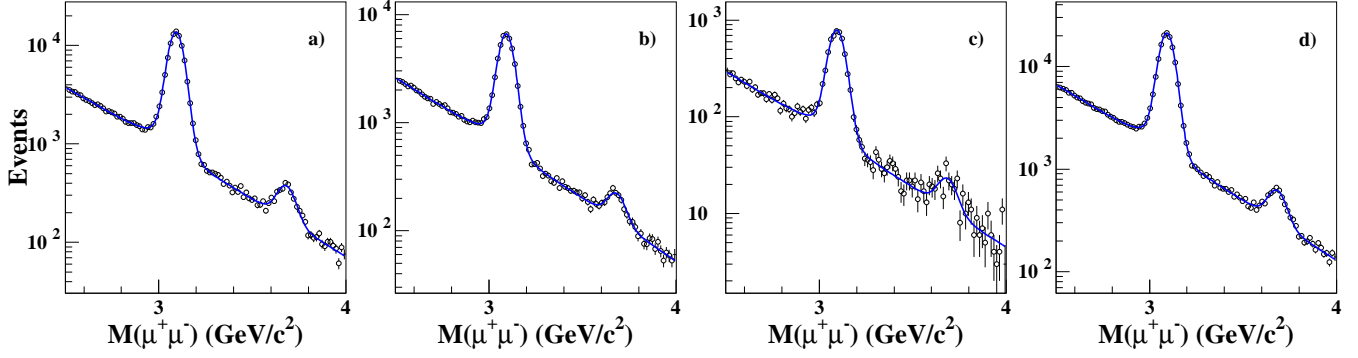


FIG. 3:  $\mu^+\mu^-$  invariant mass spectra in the muon channel for C (a), W (b), Ti (c) and full sample (d). The bin width is  $15\text{ MeV}/c^2$ .

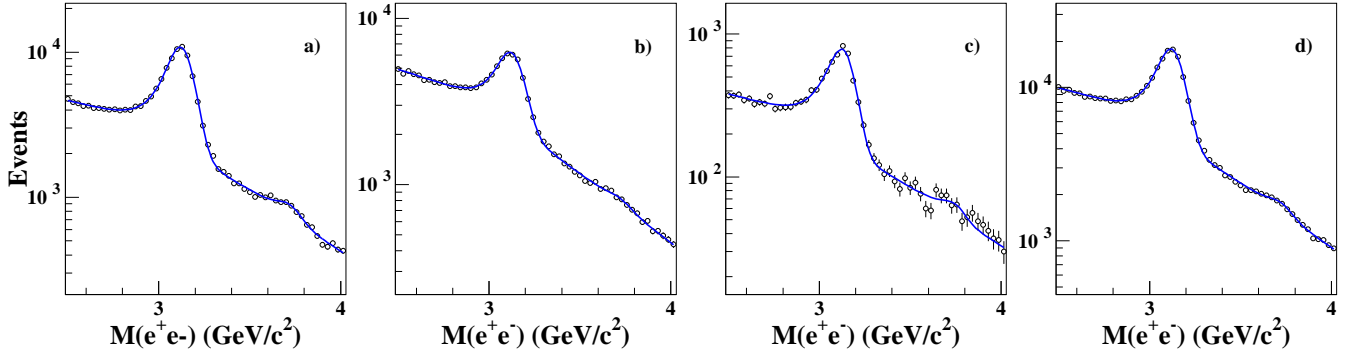


FIG. 4:  $e^+e^-$  invariant mass spectra for C (a), W (b), Ti (c) and full sample (d). The bin width is  $30\text{ MeV}/c^2$ .

Mat.	$\mu^+\mu^-$		$e^+e^-$	
	$N_{J/\psi}$	$\sigma_{J/\psi}$ ( $\text{MeV}/c^2$ )	$N_{J/\psi}$	$\sigma_{J/\psi}$ ( $\text{MeV}/c^2$ )
C	$80400 \pm 300$	$35.6 \pm 0.2$	$50030 \pm 530$	$64.2 \pm 0.8$
W	$47750 \pm 200$	$36.0 \pm 0.3$	$23460 \pm 480$	$66.1 \pm 1.6$
Ti	$4700 \pm 70$	$37.1 \pm 0.7$	$3530 \pm 150$	$58.8 \pm 2.8$
Tot	$122900 \pm 400$	$35.8 \pm 0.1$	$77020 \pm 700$	$64.3 \pm 0.8$

TABLE VI: Total numbers of  $J/\psi$  events per target material and for the full data set in the  $\mu^+\mu^-$  and  $e^+e^-$  channels.

Mat.	1-G fit	2-G fit			
		$\mu^+\mu^-$			
	$N_{\chi_c}$	$N_{\chi_{c1}+\chi_{c2}}$	$\frac{N_{\chi_{c1}}}{N_{\chi_{c2}}}$	$\sigma(\chi_{c1})$ ( $\text{GeV}/c^2$ )	
C	$6280 \pm 510$	$6390 \pm 420$	$1.20 \pm 0.26$	0.030	
W	$3120 \pm 560$	$2830 \pm 330$	$1.26 \pm 0.52$	0.032	
Ti	$390 \pm 110$	$390 \pm 110$	$0.63 \pm 0.63$	0.030	
Tot	$9570 \pm 710$	$9630 \pm 550$	$1.19 \pm 0.24$	0.031	
	$N_{\chi_c}$	$N_{\chi_{c1}+\chi_{c2}}$	$\frac{N_{\chi_{c1}}}{N_{\chi_{c2}}}$	$e^+e^-$	
				$\sigma(\chi_{c1})$ ( $\text{GeV}/c^2$ )	
C	$3890 \pm 480$	$3600 \pm 390$	$0.79 \pm 0.31$	0.032	
W	$2080 \pm 370$	$1870 \pm 330$	$0.71 \pm 0.48$	0.034	
Tot	$5630 \pm 660$	$5250 \pm 500$	$0.76 \pm 0.28$	0.033	

TABLE VII: Results of the fit of the  $\chi_c$  signal in the  $\mu^+\mu^-$  and  $e^+e^-$  channels. See text for the meaning of the different fit procedures.

available for this analysis of  $\chi_c$  production does not allow a determination of the polarisation of the  $\chi_c$  states because of large backgrounds. In the following we discuss angular distributions for the decay products of  $\chi_c$  and directly produced  $J/\psi$  states with the goal of investigating the possible influences of polarisation on the acceptances and thus on the determination of the  $\chi_c$  rates.

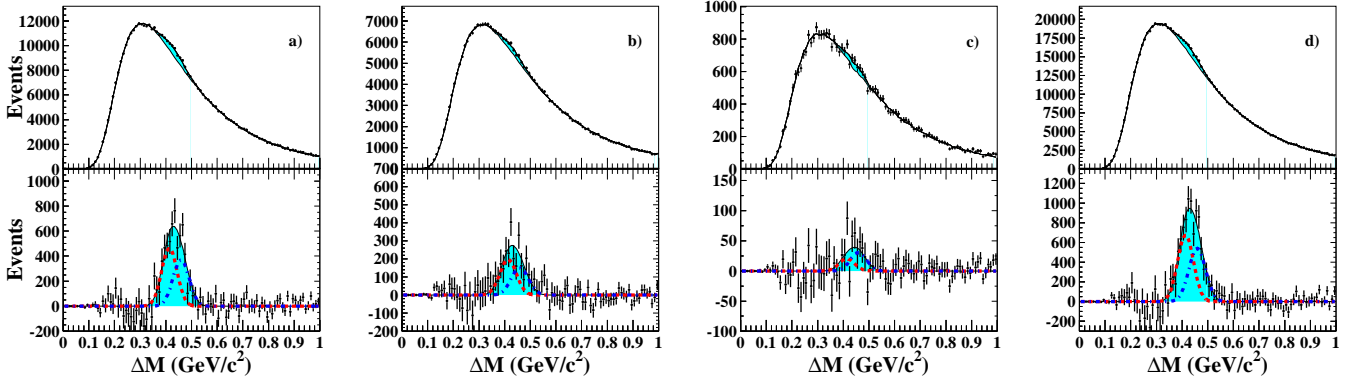


FIG. 5:  $\Delta M$  spectra in the muon channel for C (a), W (b), Ti (c) and full sample (d). The bin width is  $10\text{MeV}/c^2$ . In the background subtracted spectra the broken curves are the fitted  $\chi_{c1}$  and  $\chi_{c2}$  states.

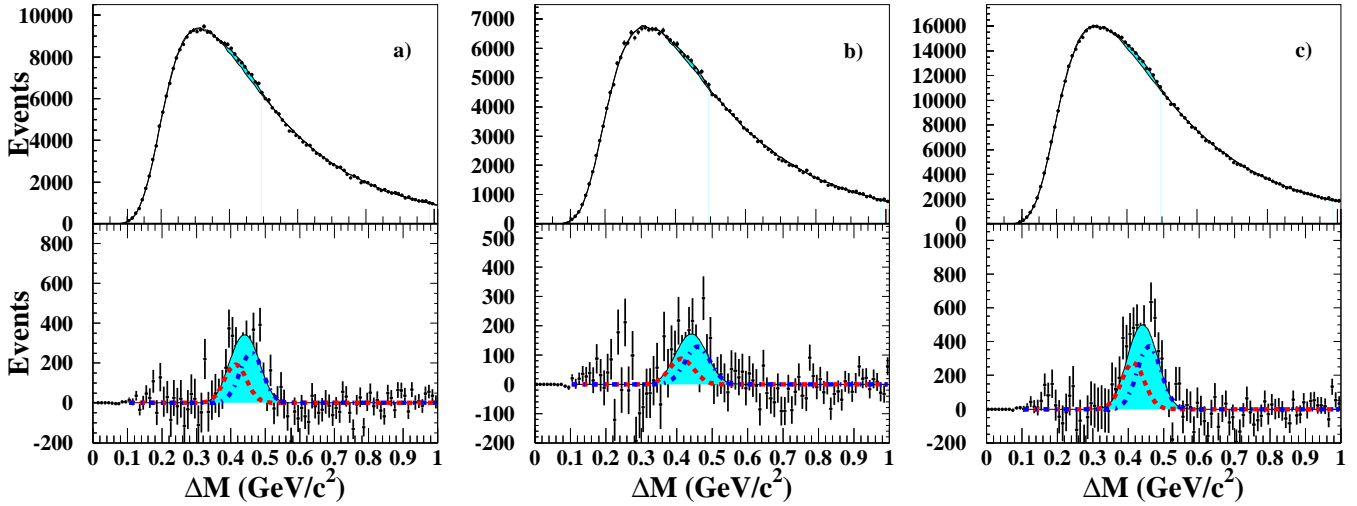


FIG. 6:  $\Delta M$  spectra in the electron channel for C (a), W (b) and full sample (c). The Ti spectrum is not shown due to the low statistics. The bin width is  $10\text{ MeV}/c^2$ . In the background subtracted spectra the broken curves are the fitted  $\chi_{c1}$  and  $\chi_{c2}$  states.

### A. $\chi_c$ polarisation

The full angular distribution of final state particles in the radiative decay

$$\chi_{cJ} \rightarrow \gamma J/\psi \rightarrow \gamma l^+ l^- \quad (6)$$

can be found for pure  $\chi_c$  polarisation states  $|J, M\rangle$  with  $J = 1, 2$  and  $|M| = 0, \dots, J$  in the appendix. The angular distribution formulae are independent of the choice of a particular polarisation axis (e. g. Gottfried-Jackson, Collins-Soper or other systems can be used). Possible coherent mixtures are not considered here because we assume that a study of the pure states will be sufficient to determine systematic acceptance effects due to polar-

isation.

If one assumes no azimuthal dependence for the production process, the  $\chi_c$  decay depends on three angles which are chosen as follows: a polar decay angle,  $\theta$ , defining the direction of the  $J/\psi$  in the  $\chi_c$  rest system with respect to the polarisation direction; a polar angle,  $\theta'$ , defining the direction of the positive lepton in the  $J/\psi$  rest system with respect to the  $J/\psi$  direction (in the  $\chi_c$  rest system); an azimuth angle,  $\phi'$ , which is the angle between the plane defined by the polarisation axis and the  $J/\psi$  direction, and the decay plane of the  $J/\psi$ .

For a state  $|J, M\rangle$  the angular distribution can be decomposed into terms with trigonometric expressions

$T_i^J(\theta, \theta', \phi')$  and coefficients  $K_i^{J,M}$  [43]:

$$W^{J,M}(\theta, \theta', \phi') = \sum_i K_i^{J,M} T_i^J(\theta, \theta', \phi'). \quad (7)$$

The angular functions  $T_i^J(\theta, \theta', \phi')$  and the coefficients  $K_i^{J,M}$ , expressed in terms of helicity amplitudes, are reported in Table X in the appendix. With the additional assumption that for both  $\chi_c$  states only the leading multipole, the electric dipole, contributes to the radiative decay, the coefficients  $K_i^{J,M}$  are uniquely defined (see appendix for the numerical values). The assumption that higher order multipoles can be neglected is well justified by experimental results [5]. The pure  $\chi_c$  polarisation states are thus unambiguously defined.

## B. $J/\psi$ polarisation

### 1. $J/\psi$ angular distributions

In leptonic  $J/\psi$  decays, the  $J/\psi$  polarisation can be determined from the angular distribution of the leptons. After integrating over the azimuthal orientation of the decay plane of the  $J/\psi$  (or assuming azimuthal symmetry) the distribution of the polar decay angle  $\theta'$  can be parameterised as:

$$\frac{1}{N} \frac{dN}{d\cos\theta'} = a(\lambda)(1 + \lambda \cos^2\theta'), a(\lambda) = \frac{1}{2(1 + \lambda/3)}, \quad (8)$$

where  $\theta'$  is the angle between the  $l^+$  and the quantisation axis. The form of the distribution (8) is independent of the chosen quantisation axis (in general however the value of  $\lambda$  is dependent on this choice).

### 2. $J/\psi$ polarisation measurement

A measurement of  $J/\psi$  polarisation by the HERA-B collaboration is reported in [44]. However the  $J/\psi$  sample used for this study includes not only directly produced  $J/\psi$  but also  $J/\psi$  from  $\chi_c$  and it is not possible to distinguish between the two contributions. Therefore the  $\lambda$ -value derived from the observed distribution,  $\lambda_{obs}$ , has to be considered as the average  $J/\psi$  polarisation parameter, independent of the origin.

The polarisation parameters have been determined using as quantisation axis, the bisector of the angle between  $\mathbf{p}_b$  and  $\mathbf{p}_t$ , where  $\mathbf{p}_b$ ,  $\mathbf{p}_t$  are the momenta of the beam proton and the target nucleon, respectively, in the  $J/\psi$  centre-of-mass system ('Collins-Soper frame'). The experimental value of the polarisation parameter, averaged over the muon and the electron decay channels and on the target materials, and assuming no dependence on  $p_T^{J/\psi}$  and  $x_F^{J/\psi}$  in the HERA-B acceptance, is [44]:

$$\lambda_{obs} = -0.35 \pm 0.04. \quad (9)$$

## C. Method for the evaluation of systematic uncertainties due to polarisation

In this section we explain the method used to estimate the systematic uncertainties for  $R_{\chi_c}$  and  $R_{12}$  arising from possible polarisations of the  $\chi_c$  and directly produced  $J/\psi$  states. The only experimental constraint which can be used for these estimations is the measured  $\lambda_{obs}$  (section VII B 2).

### 1. Principle of the method

The efficiencies entering in the formulae for  $R_{\chi_c}$  and  $R_{12}$  (3, 4) depend in general on the polarisation of the  $\chi_c$  and the directly produced  $J/\psi$  states. The efficiencies will be evaluated for the  $\chi_c$  pure polarisation states described in section VII A which will then be used to limit the ranges of possible  $R_{\chi_c}$  and  $R_{12}$  values which will in turn be used to determine the uncertainties of these values in section VIII B. As in the  $J/\psi$  analysis [44], we evaluate the polarisation states in the Collins-Soper frame. Despite this specific choice and the restriction to pure polarisation states, we assume to get an estimate of uncertainties induced by polarisation.

The formulae for  $R_{\chi_c}$  and  $R_{12}$  require the detection efficiency for direct  $J/\psi$  production  $\varepsilon_{J/\psi}^{dir}$  which depends on the polarisation parameter  $\lambda_{dir}$ . Since the observed polarisation,  $\lambda_{obs}$ , also includes the effect of possible  $\chi_c$  polarisation,  $\lambda_{dir}$  has to be disentangled from it using the values  $\lambda_1$  and  $\lambda_2$  obtained for the assumed polarisation states of  $\chi_{c1}$  and  $\chi_{c2}$  respectively. This is done with an iterative procedure in which the yet-to-be-determined values of  $R_{\chi_c}$  and  $R_{12}$  are used as inputs.

### 2. Determination of $\lambda_{dir}$ , $\lambda_1$ , $\lambda_2$

Starting from Eq. (8) the observed polar decay angle distribution can be decomposed into contributions from directly produced  $J/\psi$  and  $J/\psi$  from  $\chi_{c1}$  and  $\chi_{c2}$  events:

$$a_{obs}(1 + \lambda_{obs} \cos^2\theta') = \sum_{i=dir,1,2} f_i a_i (1 + \lambda_i \cos^2\theta'), \quad (10)$$

with  $a_i = a(\lambda_i)$ . The fractions  $f_i$  ( $i = dir, 1, 2$ ) of the different types of  $J/\psi$  are determined by  $R_{\chi_c}$  and  $R_{12}$ . With  $\sum_i f_i = 1$ ,  $f_1 + f_2 = R_{\chi_c}$  and  $f_1/f_2 = R_{12}$  one obtains

$$f_{dir} = 1 - R_{\chi_c}, \quad f_1 = \frac{R_{\chi_c} R_{12}}{1 + R_{12}}, \quad f_2 = \frac{R_{\chi_c}}{1 + R_{12}}. \quad (11)$$

Since there is no direct measurement of  $\lambda_1$  and  $\lambda_2$ , the angular distributions corresponding to the different pure polarisation states  $|J, M\rangle$  of  $\chi_{c1}$  and  $\chi_{c2}$  described in Sect. VII A are used to determine the sub-ranges allowed for  $\lambda_1$  and  $\lambda_2$ , out of the full  $[-1.0, 1.0]$  interval. For this purpose, the unpolarised  $\chi_c$  angular distribution

is re-weighted with the corresponding function (7). The resulting  $\cos \theta'$  distribution is then fitted with the function (8) which then yields  $\lambda_1$  or  $\lambda_2$  corresponding to the tested pure  $\chi_c$  polarisation state.

Solving (10) for  $\lambda_{dir}$  as a function of  $\lambda_{obs}$  for given values of  $\lambda_1$ ,  $\lambda_2$ ,  $R_{\chi_c}$  and  $R_{12}$  yields:

$$\lambda_{dir}(\lambda_{obs} | \lambda_1, \lambda_2, R_{\chi_c}, R_{12}) = \frac{a_{obs} \lambda_{obs} - a_1 f_1 \lambda_1 - a_2 f_2 \lambda_2}{a_{obs} - a_1 f_1 - a_2 f_2}. \quad (12)$$

In this equation  $R_{\chi_c}$  and  $R_{12}$  enter via the fractions  $f_i$ . On the other hand, as both depend also on  $\lambda_{dir}$ , an iterative procedure is applied starting with  $\lambda_{dir} = 0$ .

### 3. Polarisation dependence of the efficiencies

For each tested pure  $\chi_c$  polarisation state with the corresponding set of values  $\lambda_{dir}$ ,  $\lambda_1$ ,  $\lambda_2$ , new efficiencies  $\varepsilon_\gamma$  and  $\varepsilon_{J/\psi}$  are determined.

*a.  $J/\psi$  efficiencies:* Assuming no dependence of  $\lambda$  on  $x_F^{J/\psi}$  and  $p_T^{J/\psi}$  (approximately valid within the uncertainty of our measurement [44]), we can write  $\varepsilon_{J/\psi}(\lambda)$  as:

$$\varepsilon_{J/\psi}(\lambda) = \frac{N_{reco}^{J/\psi}}{N_{gen}^{J/\psi}} = \frac{\int A(\cos \theta', P) \cdot M(P) \cdot (1 + \lambda \cos^2 \theta') \cdot d \cos \theta' dP}{\int M(P) \cdot (1 + \lambda \cos^2 \theta') \cdot d \cos \theta' dP}, \quad (13)$$

where  $\theta'$  is the polar angle in the polarisation frame,  $P$  is shorthand for all the other phase space variables,  $A(\cos \theta', P)$  is the acceptance at the kinematical point  $(\cos \theta', P)$ ,  $M(P)$  is the squared matrix element in  $P$  and  $\lambda$  is the polarisation parameter. After calculating the integrals we find:

$$\varepsilon_{J/\psi}(\lambda) = \varepsilon_{J/\psi}(\lambda = 0) \frac{1 + \lambda \cdot \langle \cos^2 \theta' \rangle}{(1 + \lambda/3)}, \quad (14)$$

where  $\langle \cos^2 \theta' \rangle$  is given by:

$$\langle \cos^2 \theta' \rangle = \frac{\int A(\cos \theta', P) \cdot M(P) \cdot \cos^2 \theta' \cdot d \cos \theta' dP}{\int A(\cos \theta', P) \cdot M(P) \cdot d \cos \theta' dP}.$$

All  $J/\psi$  efficiencies, both for direct  $J/\psi$  and for  $J/\psi$  from the two  $\chi_c$  states, are calculated using Eq. 14.

*b. Photon efficiencies:* To determine the effect of polarisation on the photon efficiencies we start with the formula:

$$\varepsilon_\gamma^{\chi_{cJ}} = \frac{N_{\chi_{cJ}, M}}{N_{J/\psi}^{\chi_{cJ}, M}}, \quad (15)$$

where  $J, M$  denotes the polarisation state considered,  $N_{J/\psi}^{\chi_{cJ}, M}$  is the number of  $J/\psi$  coming from  $\chi_{cJ}$  and  $N_{\chi_{cJ}, M}$  is the number of observed  $\chi_{cJ}$ . The value of

$N_{J/\psi}^{\chi_{cJ}, M}$  is obtained from a fit of the  $l^+ l^-$  mass distribution, where each event enters with a weight:

$$w(\cos \theta', \lambda_{J, M}) = \frac{1 + \lambda_{J, M} \cdot \cos^2 \theta'}{(1 + \lambda_{J, M}/3)}. \quad (16)$$

The value of  $N_{\chi_{cJ}, M}$  is obtained from a fit of the  $\Delta M$  distribution of true  $\chi_{cJ}$  (using MC generator information to select the correct  $J/\psi\gamma$  combination), where the weight for each entry in the histogram corresponds to a certain pure polarisation state of  $\chi_{cJ}$ , calculated by Eq. 7.

## VIII. SYSTEMATIC UNCERTAINTIES

### A. Uncertainties from reconstruction, calibration, simulation and background subtraction

With the exception of  $J/\psi$  counting, all of the systematic uncertainties in the measurement of  $R_{\chi_c}$  are common to the  $e^+ e^-$  and  $\mu^+ \mu^-$  channels. The  $J/\psi$  counting systematic uncertainties are estimated to be 2% in the electron channel and 0.25% in the muon channel.

The remaining systematic uncertainty estimates include:

#### $\chi_c$ counting:

- photon selection (7%);
- variation of  $l^+ l^-$  mass window (2%);
- $\chi_c$  counting procedure (4%) including:
  - variation of the fixed parameters of the double-gaussian fit:  $\Delta M_{\chi_{c1}}$ ,  $\sigma_{\chi_{c1}}$ ,  $\Delta M(\chi_{c2}) - \Delta M(\chi_{c1})$  and  $\frac{\sigma_{\chi_{c2}}}{\sigma_{\chi_{c1}}}$ ;
  - fit with free  $\Delta M_{\chi_{c1}}$  and/or  $\sigma_{\chi_{c1}}$ ;
  - change of binning of the  $\Delta M$  spectrum.
- Extensive tests were performed on the background determination with the mixed event procedure:
  - variation of corrections corresponding to combinations of  $J/\psi$ 's with photons from  $\chi_c$  decays in ME which do not occur in SE (+3%);
  - relaxing the requirement of the same neutral cluster multiplicity in ME and SE ( $\pm 2\%$ );
  - variation of the cut on the neutral cluster direction in ME with respect to SE ( $\pm 3\%$ );
  - allowing for an additional, polynomial term in the background to improve the fit around the  $\chi_c$  signal yields an asymmetric uncertainty (+4%).

The total contribution from the background description to the systematic uncertainty in the  $\chi_c$  counting is estimated to range between -4% and +6%.

## Efficiency evaluation

- the use of different kinematic distributions for the generation of the  $J/\psi$  (see Ref. [28] and [37]), affecting both  $\frac{\varepsilon_{J/\psi}^{\chi_c}}{\varepsilon_{J/\psi}^{dir}}$  and  $\varepsilon_\gamma$ , introduces a systematic effect on  $R_{\chi_c}$  of 4%;
- tests on the photon efficiency simulation were performed including the comparison between real data and Monte Carlo of the  $\gamma$  conversion yield and of the detection efficiency of photons from electron Bremsstrahlung. The overall systematic uncertainty on  $\varepsilon_\gamma$  determination and correction is found to be 6.5%.

The overall systematic uncertainty on  $R_{\chi_c}$ , evaluated as the quadratic sum of the above terms, is therefore  $+13\%$  for both  $J/\psi$  decay channels.

The systematic uncertainty on  $R_{12}$  is completely dominated by the accuracy of the ECAL energy calibration which affects  $\Delta M(\chi_{c1})$  which in turn affects the ratio  $\frac{N_{\chi_{c1}}}{N_{\chi_{c2}}}$ . A fine tuning of the ECAL calibration as a function of the photon energy was performed using the  $\pi^0 \rightarrow \gamma\gamma$  signal. An absolute calibration accuracy of  $\sim 2\%$  was obtained and on  $\Delta M_{\chi_{c1}}$  of  $\sim 8$  MeV/ $c^2$ . By scanning  $\Delta M(\chi_{c1})$  in such range around the nominal value [5], a variation of  $\frac{N_{\chi_{c1}}}{N_{\chi_{c2}}}$  (and thus  $R_{12}$ ) of 35% is obtained. No effect on  $R_{12}$  is observed by changing the other fixed fit parameters.

## B. Polarisation effects

Since the direct  $J/\psi$  and  $\chi_c$  polarisations cannot be determined separately from our data, we estimate instead systematic uncertainties on the reference values reported in Table VIII (and denoted by  $R_{\chi_c}^{ref}$  and  $R_{12}^{ref}$  in the following) which were obtained with the assumption of zero polarisation. The results of this study are expressed as overall shifts of the values of  $R_{\chi_c}$  and  $R_{12}$  due to the average polarisation of directly produced  $J/\psi$  with uncertainties obtained from the maximum variation of  $\chi_c$  polarisations allowed by the measurement:

$$\begin{aligned} \frac{R_{\chi_c} - R_{\chi_c}^{ref}}{R_{\chi_c}^{ref}} &= +9.5\%_{-7\%}^{+11\%} \\ \frac{R_{12} - R_{12}^{ref}}{R_{12}^{ref}} &= +0\%_{-11\%}^{+16\%}, \end{aligned} \quad (17)$$

where the following ingredients are used:

- The central values are obtained from the average measured value for  $\lambda_{obs}$  and with the assumption of no polarisation of  $\chi_{c1}$  and  $\chi_{c2}$  ( $\lambda_{obs} = -0.35$ ,  $\lambda_1 = 0$  and  $\lambda_2 = 0$ , yielding  $\lambda_{dir} = -0.424$ ). Therefore, if the observed  $J/\psi$  polarisation were due exclusively to direct  $J/\psi$  polarisation, the measured  $R_{\chi_c}$  would be shifted up by 9.5%, while obviously no effect on  $R_{12}$  is produced.

- The variation bands in Eq. 17 are obtained by taking the extreme positive and negative variations of the central values defined above, of all combinations of  $\lambda_{obs}$  (varied in a 95% c.l. range around the measured value, see Eq. 9) with  $\lambda_1$  and  $\lambda_2$  (corresponding to the different pure helicity states M1 and M2):

- upper value:  $\lambda_{obs} = -0.44$ ;  $\lambda_1 = -0.24$ ,  $\lambda_2 = 0.18$  for  $R_{\chi_c}$ ;  $\lambda_1 = -0.24$ ,  $\lambda_2 = -0.18$  for  $R_{12}$ ;
- lower value:  $\lambda_{obs} = -0.26$ ;  $\lambda_1 = 0.22$  and  $\lambda_2 = -0.18$  for  $R_{\chi_c}$ ;  $\lambda_1 = 0.22$  and  $\lambda_2 = 0.18$  for  $R_{12}$ .

- Different polarisation values give overlapping ranges of possible  $R_{\chi_c}$  and  $R_{12}$  values. Any value in each range is equally probable. Thus, even if the error on  $\lambda_{obs}$  was Gaussian distributed, the errors of  $R_{\chi_c}$  and  $R_{12}$  would not be Gaussian distributed. To take into account that the polarisation parameter  $\lambda_{obs}$  was determined as an average over the whole accepted phase space and over different materials,  $\lambda_{obs}$  was varied in a  $\pm 2\sigma$  range with equal weights. Selecting the maximum deviations the measured values  $R_{\chi_c}$  and  $R_{12}$  would have to be scaled:

$$R_{\chi_c} = f_{R_{\chi_c}} \cdot R_{\chi_c}^{ref} \quad (18)$$

$$R_{12} = f_{R_{12}} \cdot R_{12}^{ref},$$

with  $f_{R_{\chi_c}} \in [1.02, 1.21]$  and  $f_{R_{12}} \in [0.89, 1.16]$ , where the uncertainties due to polarization are fully contained in the ranges given.

- Note that the correlation between the values of  $R_{\chi_c}$  and  $R_{12}$  are ignored in Eqs. 17 and 18.

## IX. RESULTS

### A. $R_{\chi_c}$

The measured values for  $R_{\chi_c}$  are computed from Eq. 3, assuming zero  $J/\psi$  polarisation and are reported in Tab. VIII, separately for muon and electron channels and combined sample. When averaged over decay channels and target materials, a value of

$$R_{\chi_c} = 0.188 \pm 0.013_{st-0.022sys}^{+0.024} \quad (19)$$

is obtained. The quoted uncertainties include all systematic contributions (except the polarisation contribution which is given in Eq. 17 as a variation band at 95% c.l.). The following observations can be made:

- The results obtained in the two lepton channels are compatible within  $1\sigma$  in both C and W samples. No measurement for the Ti in the electron channel is possible due to the low statistics;

- The values of  $R_{\chi_c}$  obtained separately in the three target samples are consistent with each other;
- The present result is lower than most values published in the literature in pN interactions (see Tab. III and Fig. 1). Despite the fact that the various available measurements are taken at widely differing centre of mass energies, they are for the most part compatible within  $\sim 1.5\sigma$ , except for E705 ( $2.3\sigma$ ) and ISR ( $3.3\sigma$ ).

The present measurement is lower than the previous HERA-B result [14] by about  $2\sigma$ . The two analyses are quite similar, although more extensive systematic checks have been performed in connection with the present one. These checks did not uncover any error in the previous analysis and we thus believe that the differences are largely statistical. The average of the two HERA-B results,  $R_{\chi_c} = 0.198^{+0.028}_{-0.026}$ , differs by less than  $1\sigma$  from the result of Eq. 19.

## B. $R_{12}$

The measured values of  $R_{12}$  are evaluated using Eq. 4, assuming no polarisation for either the directly produced  $J/\psi$ 's or the  $\chi_c$ 's, and are summarised in Table VIII.

As above, no dependence on target material is observed. The results from the electron channel are consistently lower than the muon results, but nonetheless in agreement to within  $1\sigma$  of the statistical uncertainties.

The final result averaged over decay channel and target material is:

$$R_{12} = 1.02 \pm 0.17_{st} \pm 0.36_{sys} \quad (20)$$

where the systematic uncertainty does not include the polarisation contribution which is given in Eq. 17 as a variation band at 95% c.l. The  $J/\psi$  yields from  $\chi_{c1}$  and  $\chi_{c2}$  are therefore found to be equal, although with large uncertainties.

## C. Dependence on kinematic variables

A study of the dependence of  $R_{\chi_c}$  on the kinematic variables  $x_F^{J/\psi}$  and  $p_T^{J/\psi}$  in the ranges covered by HERA-B ( $x_F^{J/\psi} \in [-0.35, 0.15]$ ,  $p_T^{J/\psi} \lesssim 5 \text{ GeV}/c$ ) was performed by applying the described procedure in five  $x_F^{J/\psi}$  and three  $p_T^{J/\psi}$  intervals respectively. The resulting distributions, for both channels combined, are shown in Fig. 7a)-b). The data is compatible with a flat dependence of  $R_{\chi_c}$  on both kinematic variables, although more complex dependences cannot be ruled out.

## D. A-dependence

The atomic mass number (A) dependence of inclusive cross sections is often parameterised as a power law:

$$\sigma_{pA} = \sigma_{pN} A^\alpha \quad (21)$$

where  $\sigma_{pA}$  is the inclusive production cross section in collisions of protons with a nuclear target of atomic mass number A,  $\sigma_{pN}$  is the average cross section in collisions of protons with a single nucleon and  $\alpha$  characterises the A dependence of the cross section. The difference between  $\alpha$  for  $J/\psi$  production and that for  $\chi_c$  production can be computed from the measured values of  $R_{\chi_c}$  for C and W targets given in Tab. VIII from the following formula:

$$\Delta\alpha = \alpha_{\chi_c} - \alpha_{J/\psi} = \frac{1}{\log \frac{A_W}{A_C}} \cdot \log \frac{R_{\chi_c}^W}{R_{\chi_c}^C} \quad (22)$$

where  $A_W = 184$  and  $A_C = 12$  are the tungsten and carbon atomic mass numbers. The results, plotted as a function of  $x_F^{J/\psi}$  and  $p_T^{J/\psi}$  are shown in Figs. 7c), d). Averaged over the visible  $x_F^{J/\psi}$  and  $p_T^{J/\psi}$  range,  $\Delta\alpha = 0.05 \pm 0.04$ . The predictions of the various production models for  $\Delta\alpha$  are all within the uncertainties of the measurement [22].

## E. $\chi_c$ cross sections and ratio

From Eq. 5 we obtain the values for the cross section ratio  $\frac{\sigma(\chi_{c1})}{\sigma(\chi_{c2})}$  under the assumption of zero polarisation for both  $J/\psi$  and  $\chi_c$ . The results are reported in Tab. VIII. The target material averaged result is:

$$\frac{\sigma(\chi_{c1})}{\sigma(\chi_{c2})} = 0.57 \pm 0.23 \quad (23)$$

where the uncertainty includes the systematic contributions (except polarisation - see above). The  $\chi_c$  production cross sections, defined as:

$$\sigma(\chi_{ci}) = \frac{\sigma(J/\psi) R_{\chi_{ci}}}{Br(\chi_{ci} \rightarrow J/\psi \gamma)}, i = 1, 2 \quad (24)$$

are calculated using the estimate of the total  $J/\psi$  cross section at  $\sqrt{s} = 41.6 \text{ GeV}$ ,  $\sigma(J/\psi) = (502 \pm 44) \text{ nb/nucleon}$  reported in [29] and assuming that  $R_{\chi_c}$  is independent of  $x_F^{J/\psi}$  over the full  $x_F^{J/\psi}$  and  $p_T^{J/\psi}$  range. The following target material averaged values are obtained:

$$\begin{aligned} \sigma(\chi_{c1}) &= 133 \pm 35 \text{ nb/nucleon;} \\ \sigma(\chi_{c2}) &= 231 \pm 61 \text{ nb/nucleon.} \end{aligned} \quad (25)$$

leading to a total  $\chi_c$  production cross section  $\sigma(\chi_c) = 364 \pm 74 \text{ nb/nucleon}$ . Fig. 1 shows all available measurements of the  $\chi_{c1}$  and  $\chi_{c2}$  production cross sections and their ratio in proton-nucleus interactions at fixed-target energies.

Mat.	$e^+e^-$	$\mu^+\mu^-$	combined
$R_{\chi_c}$			
C	$0.174 \pm 0.029_{st}^{+0.022}_{-0.021_{sys}}$	$0.190 \pm 0.018_{st}^{+0.024}_{-0.022_{sys}}$	$0.185 \pm 0.015_{st}^{+0.024}_{-0.022_{sys}}$
Ti	-	$0.197 \pm 0.079_{st}^{+0.025}_{-0.023_{sys}}$	$0.197 \pm 0.079_{st}^{+0.025}_{-0.023_{sys}}$
W	$0.202 \pm 0.055_{st}^{+0.026}_{-0.024_{sys}}$	$0.191 \pm 0.034_{st}^{+0.025}_{-0.022_{sys}}$	$0.194 \pm 0.029_{st}^{+0.025}_{-0.023_{sys}}$
Tot	$0.180 \pm 0.025_{st}^{+0.023}_{-0.021_{sys}}$	$0.190 \pm 0.015_{st}^{+0.024}_{-0.022_{sys}}$	$0.188 \pm 0.013_{st}^{+0.024}_{-0.022_{sys}}$
$R_{12}$			
C	$0.82 \pm 0.32_{st}$	$1.23 \pm 0.27_{st}$	$1.06 \pm 0.21_{st} \pm 0.37_{sys}$
Ti	-	$0.67 \pm 0.67_{st}$	$0.67 \pm 0.67_{st} \pm 0.23_{sys}$
W	$0.73 \pm 0.49_{st}$	$1.27 \pm 0.53_{st}$	$0.98 \pm 0.36_{st} \pm 0.34_{sys}$
Tot	$0.79 \pm 0.27_{st}$	$1.17 \pm 0.22_{st}$	$1.02 \pm 0.17_{st} \pm 0.36_{sys}$
$\frac{\sigma(\chi_{c1})}{\sigma(\chi_{c2})}$			
C	$0.47 \pm 0.19_{st}$	$0.70 \pm 0.16_{st}$	$0.60 \pm 0.12_{st} \pm 0.21_{sys}$
Ti	-	$0.38 \pm 0.38_{st}$	$0.38 \pm 0.38_{st} \pm 0.13_{sys}$
W	$0.41 \pm 0.28_{st}$	$0.72 \pm 0.30_{st}$	$0.56 \pm 0.21_{st} \pm 0.20_{sys}$
Tot	$0.45 \pm 0.16_{st}$	$0.66 \pm 0.13_{st}$	$0.57 \pm 0.10_{st} \pm 0.20_{sys}$

TABLE VIII: Measured values of  $R_{\chi_c}$ ,  $R_{12}$  and  $\frac{\sigma(\chi_{c1})}{\sigma(\chi_{c2})}$  in  $e^+e^-$ ,  $\mu^+\mu^-$  and combined sample for the different materials and the full data sample.

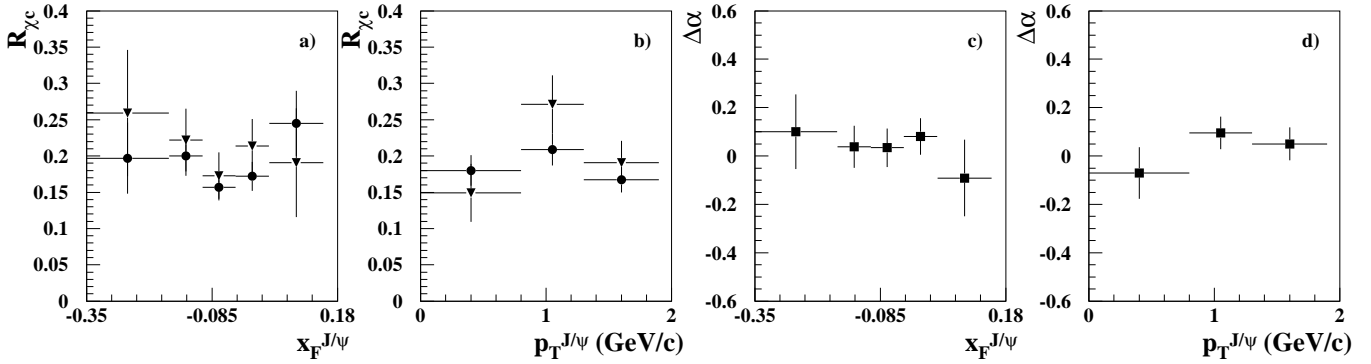


FIG. 7: Dependence of  $R_{\chi_c}$  on  $x_F^{J/\psi}$  (a) and  $p_T^{J/\psi}$  (b) (circles: C; triangles: W). Dependence of  $\Delta\alpha = \alpha_{\chi_c} - \alpha_{J/\psi}$  on  $x_F^{J/\psi}$  (c) and  $p_T^{J/\psi}$  (d). Only statistical errors are shown.

## X. CONCLUSION

We have presented a new measurement of the fraction of all  $J/\psi$  mesons produced through  $\chi_c$  decay ( $R_{\chi_c}$ ), performed with the HERA-B detector in pC, pTi and pW interactions at  $920 \text{ GeV}/c$  ( $\sqrt{s} = 41.6 \text{ GeV}$ ). The  $\chi_c$  mesons were detected in the  $J/\psi\gamma$  decay mode, and the  $J/\psi$  in both  $\mu^+\mu^-$  and  $e^+e^-$  decay modes. The detector acceptance was flat in  $p_T^{J/\psi}$  and extended from  $x_F^{J/\psi} = -0.35$  to  $x_F^{J/\psi} = 0.15$ .

The measurement is based on a total sample of  $\sim 15000$   $\chi_c$ , the largest ever observed in pA collisions. Apart from lepton identification requirements, the analysis is identical for the two channels. The separate results for the two channels are found to be in agreement with each other in all respects.

The measured value  $R_{\chi_c} = 0.188 \pm 0.013_{st}^{+0.024}_{-0.022_{sys}}$  is  $\sim 2\sigma$  lower than the previously published result from HERA-B. Our new value is also lower than, but not incompatible with, most of the previously published values obtained from pN interactions, independent of the centre of mass energies and the kinematic ranges of the measurements. The present result supports the NRQCD calculations [22]. When taken together with the already published result of HERA-B on  $\psi'$  production [28], the fraction of all  $J/\psi$  mesons coming from decays of higher mass charmonium states is found to be  $\sim 27\%$ .

By separately counting the contribution of  $\chi_{c1}$  and  $\chi_{c2}$ , we obtain a ratio of the two states  $R_{12} = R_{\chi_{c1}}/R_{\chi_{c2}} = 1.02 \pm 0.40$  and a cross section ratio  $\frac{\sigma(\chi_{c1})}{\sigma(\chi_{c2})} = 0.57 \pm 0.23$ . The  $\chi_{c1}$  and  $\chi_{c2}$  cross sections are measured to be  $\sigma(\chi_{c1}) = 133 \pm 35 \text{ nb/nucleon}$  and  $\sigma(\chi_{c2}) = 231 \pm$



61 nb/nucleon in the full  $x_F^{J/\psi}$  range.

No significant departure from a flat dependence of  $R_{\chi_c}$  on the kinematic variables  $x_F^{J/\psi}$  and  $p_T^{J/\psi}$  is found within the limited accuracy of our measurement. No significant difference in the A-dependence of  $\chi_c$  and  $J/\psi$  production is found within the limits of the available statistics.

For the first time, an evaluation of the effect of polarisation of  $J/\psi$  and  $\chi_c$  on the measured values of  $R_{\chi_c}$  and  $R_{12}$  was performed. The behaviour of  $R_{\chi_c}$  and  $R_{12}$  as a function of the polarisation, expressed by the  $\lambda$  parameter, was studied with the conclusion that  $R_{\chi_c}$  and  $R_{12}$  are uncertain with factors in the ranges [1.02,1.21] and [0.89,1.16], respectively, ignoring correlations between the two.

No mention of the influence of polarisation on the measurement of  $R_{\chi_c}$  can be found in any of the previous measurements. Nonetheless, we suspect that all measurements are subject to similar uncertainties to greater or lesser extents, depending on the geometry of the apparatus used.

## XI. ACKNOWLEDGEMENTS

We express our gratitude to the DESY laboratory for the strong support in setting up and running the HERA-B experiment. We are also indebted to the DESY accelerator group for the continuous efforts to provide good and stable beam conditions. The HERA-B experiment would not have been possible without the enormous effort and commitment of our technical and administrative staff. It is a pleasure to thank all of them.

## APPENDIX A: $\chi_c$ ANGULAR DISTRIBUTIONS

The angular decay distribution of a pure polarisation state  $|J, M\rangle$  is given as an expansion into helicity amplitudes  $A_{|\nu|}^J$  by [43]:

$$W^{J,M}(\theta, \theta', \phi') = \sum_{\nu, \nu'=-J}^{+J} \sum_{\mu=\pm 1} d_{M\nu}^J(\theta) d_{M\nu'}^{J*}(\theta) A_{|\nu|}^J \rho^{\sigma\sigma'}(\theta', \phi') \quad (\text{A1})$$

with the density matrix for the  $J/\psi$  helicity (IX):

$$\rho^{\sigma\sigma'}(\theta', \phi') = \sum_{\kappa=\pm 1} D_{\sigma\kappa}^1(\phi', \theta', -\phi') D_{\sigma'\kappa}^{1*}(\phi', \theta', -\phi'). \quad (\text{A2})$$

Using the notation of [43] the angular distribution can be decomposed into terms with trigonometric expressions  $T_i^J(\theta, \theta', \phi')$  and coefficients  $K_i^{J,M}(A_{|\nu|}^J)$ :

$$W^{J,M}(\theta, \theta', \phi') = \sum_i K_i^{J,M}(A_{|\nu|}^J) T_i^J(\theta, \theta', \phi'). \quad (\text{A3})$$

The  $K_i^{J,M}(A_{|\nu|}^J)$  and  $T_i^J(\theta, \theta', \phi')$  are reported for  $J = 1, 2$  in Table X. The normalisations are for the angular distributions

$$\int W^{J,M}(\theta, \theta', \phi') d\cos\theta d\phi d\cos\theta' d\phi' = \begin{cases} \frac{64\pi^2}{9} & \text{for } J = 1 \\ \frac{64\pi^2}{15} & \text{for } J = 2 \end{cases} \quad (\text{A4})$$

The helicity amplitudes  $A_{|\nu|}^J$  can be expanded in multipole amplitudes (E1, M2, E3), see for example [43]. With the restriction to electric dipole transitions the helicity amplitudes become:

$$J = 1 : \quad A_0 = \sqrt{\frac{1}{2}}, \quad A_1 = \sqrt{\frac{1}{2}} \quad (\text{A5})$$

$$J = 2 : \quad A_0 = \sqrt{\frac{1}{10}}, \quad A_1 = \sqrt{\frac{3}{10}}, \quad A_2 = \sqrt{\frac{3}{5}}$$

The Table X reports also the coefficients  $K_i^{J,M}$  calculated with these values for the helicity amplitudes. Hence, with the restriction to the lowest multipole, the angular distributions of a  $\chi_c$  decay for a given polarisation state  $|J, M\rangle$  is fully determined (obviously, the relative contributions of different polarisation states are not fixed).

- 
- |   |  |
|---|--|
| <p>[1] T. Matsui and H. Satz, Phys. Lett. <b>B178</b> (1986) 416.<br/> [2] R.V. Gavai <i>et al.</i>, Int. J. Mod. Phys. A10 (1995) 3043.<br/> [3] R. Baier and R. Rückl, Z. Phys. <b>C19</b> (1983) 251; G.A. Schuler, hep-ph/9403387, CERN-TH.7170/94.<br/> [4] G.T. Bodwin <i>et al.</i>, Phys. Rev. <b>D51</b> (1995) 1125; M. Beneke and I.Z. Rothstein, Phys. Rev. <b>D54</b> (1996) 2005, <i>Erratum ibid.</i>, <b>D54</b> (1996) 7082.<br/> [5] W.-M. Yao <i>et al.</i> (Particle Data Group), Review of Particle Physics, J. Phys. G <b>33</b> (2006) 1.<br/> [6] J.H. Cobb <i>et al.</i>, Phys. Lett. <b>B72</b> (1978) 497.</p> | <p>[7] R702 collab., A.G. Clark <i>et al.</i>, Nucl. Phys. <b>B142</b> (1978) 29.<br/> [8] C. Kourkoumelis <i>et al.</i>, Phys. Lett. <b>B81</b> (1979) 405.<br/> [9] E610 collab., D.A. Bauer <i>et al.</i>, Phys. Rev. Lett. <b>54</b> (1985) 753.<br/> [10] E705 collab., L. Antoniazzi <i>et al.</i>, Phys. Rev. Lett. <b>70</b> (1993) 383.<br/> [11] CDF collab., F. Abe <i>et al.</i>, Phys. Rev. Lett. <b>79</b> (1997) 578.<br/> [12] E771 collab., T. Alexopoulos <i>et al.</i>, Phys. Rev. <b>D62</b></p> |
|---|--|

$\sigma \backslash \sigma'$	-1	0	1
-1	$\frac{1+\cos^2 \theta'}{2}$	$-\frac{\sin \theta' \cos \theta'}{\sqrt{2}} e^{i\phi'}$	$\frac{\sin^2 \theta'}{2} e^{2i\phi'}$
0	$-\frac{\sin \theta' \cos \theta'}{\sqrt{2}} e^{-i\phi'}$	$\sin^2 \theta$	$\frac{\sin \theta' \cos \theta'}{\sqrt{2}} e^{i\phi'}$
1	$\frac{\sin^2 \theta'}{2} e^{-2i\phi'}$	$\frac{\sin \theta' \cos \theta'}{\sqrt{2}} e^{-i\phi'}$	$\frac{1+\cos^2 \theta'}{2}$

TABLE IX: Helicity density matrix for the  $J/\psi$  decay as defined in (IX)

J=1						
		$K_i^{1,M}$ (general)		$K_i^{1,M}$ (E1 only)		
i	$T_i^1$	$M=0$	$M=1$	$M=0$	$M=1$	
1	1	$A_1^2$	$\frac{1}{2}(A_0^2 + A_1^2)$	0.5	0.5	
2	$\cos^2 \theta$	$A_0^2 - A_1^2$	$\frac{1}{2}(-A_0^2 + A_1^2)$	0	0	
3	$\cos^2 \theta'$	$-A_1^2$	$\frac{1}{2}(A_0^2 - A_1^2)$	-0.5	0	
4	$\cos^2 \theta \cos^2 \theta'$	$A_0^2 + A_1^2$	$-\frac{1}{2}(A_0^2 + A_1^2)$	1.0	-0.5	
5	$\sin 2\theta \sin 2\theta' \cos \phi'$	$-\frac{1}{2}A_0A_1$	$\frac{1}{4}A_0A_1$	-0.25	0.125	

J=2						
		$K_i^{2,M}$ (general)		$K_i^{2,M}$ (E1 only)		
i	$T_i^2$	$M=0$	$M=1$	$M=2$	$M=0$	$M=1$ $M=2$
1	1	$\frac{1}{4}A_0^2 + \frac{3}{8}A_2^2$	$\frac{1}{2}A_1^2 + \frac{1}{4}A_2^2$	$\frac{3}{8}A_0^2 + \frac{1}{2}A_1^2 + \frac{1}{16}A_2^2$	0.25	0.3 0.225
2	$\cos^2 \theta$	$-\frac{3}{2}A_0^2 + 3A_1^2 - \frac{3}{4}A_2^2$	$\frac{3}{2}A_0^2 - \frac{3}{2}A_1^2$	$-\frac{3}{4}A_0^2 + \frac{3}{8}A_2^2$	0.3	-0.3 0.15
3	$\cos^4 \theta$	$\frac{9}{4}A_0^2 - 3A_1^2 + \frac{3}{8}A_2^2$	$-\frac{3}{2}A_0^2 + 2A_1^2 - \frac{1}{4}A_2^2$	$\frac{3}{8}A_0^2 - \frac{1}{2}A_1^2 + \frac{1}{16}A_2^2$	-0.45	0.3 -0.075
4	$\cos^2 \theta'$	$\frac{1}{4}A_0^2 + \frac{3}{8}A_2^2$	$-\frac{1}{2}A_1^2 + \frac{1}{4}A_2^2$	$\frac{3}{8}A_0^2 - \frac{1}{2}A_1^2 + \frac{1}{16}A_2^2$	0.25	0 -0.075
5	$\cos^2 \theta \cos^2 \theta'$	$-\frac{3}{2}A_0^2 - 3A_1^2 - \frac{3}{4}A_2^2$	$\frac{3}{2}A_0^2 + \frac{3}{2}A_1^2$	$-\frac{3}{4}A_0^2 + \frac{3}{8}A_2^2$	-1.5	0.6 0.15
6	$\cos^4 \theta \cos^2 \theta'$	$\frac{9}{4}A_0^2 + 3A_1^2 + \frac{3}{8}A_2^2$	$-\frac{3}{2}A_0^2 - 2A_1^2 - \frac{1}{4}A_2^2$	$\frac{3}{8}A_0^2 + \frac{1}{2}A_1^2 + \frac{1}{16}A_2^2$	1.35	-0.9 0.225
7	$\sin^2 \theta' \cos 2\phi'$	$-\frac{\sqrt{6}}{4}A_0A_2$	0	$\frac{\sqrt{6}}{8}A_0A_2$	-0.15	0 0.075
8	$\cos^2 \theta \sin^2 \theta' \cos 2\phi'$	$\sqrt{6}A_0A_2$	$-\frac{\sqrt{6}}{2}A_0A_2$	0	0.6	-0.3 0
9	$\cos^4 \theta \sin^2 \theta' \cos 2\phi'$	$-\frac{3\sqrt{6}}{4}A_0A_2$	$\frac{\sqrt{6}}{2}A_0A_2$	$-\frac{\sqrt{6}}{8}A_0A_2$	-0.45	0.3 -0.075
10	$\sin 2\theta \sin 2\theta' \cos \phi'$	$\frac{\sqrt{3}}{4}A_0A_1 + \frac{3\sqrt{2}}{8}A_1A_2$	$-\frac{\sqrt{3}}{4}A_0A_1$	$\frac{\sqrt{3}}{8}A_0A_1 - \frac{3\sqrt{2}}{16}A_1A_2$	0.3	-0.075 -0.075
11	$\cos^2 \theta \sin 2\theta \sin 2\theta' \cos \phi'$	$-\frac{3\sqrt{3}}{4}A_0A_1 - \frac{3\sqrt{2}}{8}A_1A_2$	$\frac{\sqrt{3}}{2}A_0A_1 + \frac{\sqrt{2}}{4}A_1A_2$	$-\frac{\sqrt{3}}{8}A_0A_1 - \frac{\sqrt{2}}{16}A_1A_2$	-0.45	0.3 -0.075

TABLE X: The angular distribution terms  $T_i^J(\theta, \theta', \phi')$  and the coefficients  $K_i^{J,M}(A_{|\nu|})$  as defined in (A3) for  $J = 1, 2$ . The last columns give the numerical values for the coefficients  $K_i^{J,M}$  for different  $M$  with the assumption that only the electric dipole transition contributes (see (A5)).

- (2000) 032006.
- [13] CDF collab., T. Affolder *et al.*, Phys. Rev. Lett. **86** (2001) 3963.
- [14] HERA-B collab., I. Abt *et al.*, Phys. Lett. **B561** (2003) 61.
- [15] E369 collab., T.B.W. Kirk *et al.*, Phys. Rev. Lett. **42** (1979) 619.
- [16] WA11 collab., Y. Lemoigne *et al.*, Phys. Lett. **B113** (1982) 509, *Erratum ibid.*, **B116** (1982) 470.
- [17] IHEP collab., F. Binon *et al.*, Nucl. Phys. **B239** (1984) 311.
- [18] E673 collab., S.R. Hahn *et al.*, Phys. Rev. **D30** (1984) 671.
- [19] E610 collab., D.A. Bauer *et al.*, Phys. Rev. Lett. **54** (1985) 753.
- [20] E705 collab., L. Antoniazzi *et al.*, Phys. Rev. Lett. **70** (1993) 383.
- [21] E672/706 collab., V. Koreshev *et al.*, Phys. Rev. Lett. **77** (1996) 4294.
- [22] R. Vogt, Nucl. Phys. **A700** (2002) 539.
- [23] CDF collab., A. Sansoni *et al.*, Il Nuovo Cim. A109 (1996) 827.
- [24] B. Alessandro *et al.*, Eur. Phys. J. **C39** (2005) 335.
- [25] R. Arnaldi *et al.*, Nucl. Phys. **A774** (2006) 711.
- [26] H. Buesching and H. Pereira da Costa, Nucl. Phys. **A774** (2006) 747; O. Drapier, Nucl. Phys. **A774** (2006) 325.
- [27] M. Nardi, Nucl. Phys. **A774** (2006) 353.
- [28] HERA-B collab., I. Abt *et al.*, Eur. Phys. J. **C49** (2007) 545.
- [29] F. Maltoni *et al.*, Phys. Lett. **B638** (2006) 202.
- [30] HERA-B Design Report - DESY-PRC 95/01, January 1995.
- [31] K. Ehret *et al.*, Nucl. Instr. Methods **A446** (2000) 190
- [32] C. Bauer *et al.*, Nucl. Instr. Methods **A501** (2003) 39

- [33] H. Albrecht *et al.*, Nucl. Instr. Methods **A541** (2005) 610, Nucl. Instr. Methods **A555** (2005) 310, Nucl. Instr. Methods **A576** (2007) 312.
- [34] I. Ariño *et al.*, Nucl. Instr. Methods **A516** (2004) 445.
- [35] G. Avoni *et al.*, Nucl. Instr. Methods **A580** (2007) 1209.
- [36] V. Eiges *et al.*, Nucl. Instr. Methods **A461** (2001) 104.
- [37] HERA-B collab., I. Abt *et al.*, Phys. Rev. **D73** (2006) 052005.
- [38] M. Villa *et al.*, Proceedings of VII International Conference on Calorimetry in High Energy Physics (CALOR 97), Tucson, AZ, 9-14 Nov 1997. Editors: E. Cheu, T. Embry, J. Rutherford and R. Wigmans. Singapore, World Scientific (1998) 537.
- [39] T. Sjöstrand, Comp. Phys. Comm. 82 (1994) 74.
- [40] H. Pi, Comp. Phys. Comm. 71 (1992) 173.
- [41] R. Brun *et al.*, GEANT3, CERN-DD-EE-84-1 (1987).
- [42] E866 collab., M.J. Leitch *et al.*, Phys. Rev. Lett. **84** (2000) 3256.
- [43] M.G. Olsson and C.J. Suchyta, “Radiative angular distributions from  $c\bar{c}$  states directly produced by  $p\bar{p}$  annihilation”, Phys. Rev. **D34** (1986) 2043; A.D. Martin, M.G. Olsson and W.J. Stirling, “Production and Decay of P-Wave Charmonium States in  $p\bar{p}$  Collisions”, Phys. Lett. **B147** (1984) 203.
- [44] P. Faccioli for the HERA-B collab., Nucl. Phys. **A783** (2007) e1; HERA-B collab., I. Abt *et al.*, paper in preparation.